Impact of silver ions on dielectric properties and conductivity of lithium silicate glass system mixed with red lead

T.V.N. Keerti kut[1], Sara Marijan[2], Jana Pisk[3], A. Venkata Sekhar[1], A. Siva Sesha Reddy[4], N. Venkatramaiah[5], G. Naga Raju[1], L. Pavić[2*],N. Veeraiah[1,6*]

[1]*Department of Physics, AcharyaNagarjuna University, Nagarjuna Nagar- 522 510, India*
[2]*Ruđer Bošković Institute, Division of Materials Chemistry, 10000 Zagreb, Croatia*
[3]*Department of Chemistry, Faculty of Science, University of Zagreb, Horvatovac 102a, 10000 Zagreb, Croatia*
[4]*Department of Physics, Krishna University, Machilipatnam-521004, Andhra Pradesh, India.*
[5]*Department of Chemistry, SRM Institute of Science and Technology, Kattankulathur, Chennai, Tamil Nadu, 603203, India*
[6]*Department of Physics, Andhra Loyola College (Autonomous),Vijayawada, A.P., India*

Abstract

Glasses of the composition (40-x)Li_2O-10Pb_3O_4-50SiO_2 doped with different contents of Ag_2O were fabricated and were subsequently subjected to heat-treatment. The quantitative analysis of the results of different characterization techniques indicated increasing magnitude of internal connectivity of the glass network with increasing Ag_2O content. Several dielectric parameters viz., ε', M, Z and σ_{ac}in the frequency (ω) region 0.01 Hz – 1 MHz and in the region of temperature (T) 30 ^oC–250 ^oC of these glasses were measured as functions of Ag_2O content. ε' showed a decreasing tendency with Ag_2O content which may be attributed to the decrease in the space charge polarization (scp) due to the increasing order of augmentation of glass network. Such a decrease of scp was attributed to the growing presence of PbO_4 units and also Ag^0 particles in these samples. The plots of electric modulus vs ω and T indicated relaxation character. Such relaxation phenomena were discussed in detail with the help of Cole-Cole diagrams. Probable dipoles responsible for such effects were recognized and analyzed. σ_{ac} (conductivity) exhibited a decreasing trend with Ag_2O content. The mechanism of conduction was analyzed using polaronic tunneling effect in the intermediate ω and high T ranges, whereas in the low T range it is predicted to follow QMT model. These conclusions were observed to follow the results of various spectroscopic studies. In conclusion, presence of red lead seemed to be an obstruction for the conductivity in the fast ion conducting glasses.

***Keywords*:** Red lead; Ag ions; Lithium silicate glasses; Dielectric studies; A.C. conductivity

*Corresponding authors: lpavic@irb.hr;nvr8@rediffmail.com

1. Introduction

Studies regarding the dielectric features of amorphous materials not only give the information about their insulating character but also give the information about their structural characteristics. In fact, one can monitor the conducting or non-conducting behaviour of glasses or glass ceramics by evaluating different dielectric parameters viz., ε∗ (real and imaginary dielectric constant), M*(the electric moduli), Z* (impedance) and σ_{ac}(conductivity) over broad regions of ω (frequency) and T(temperature) as a function of their composition. A number of such studies were reported on a variety of glass materials during the last several years [1-6].

Among various alkali silicate glasses, lithium oxide forms stable glasses with silicate at a high melting temperature. However, lithium mixed silicate glasses were reported to devitrify with greater ease than other alkali silicate glasses [7] and in fact fairly stable lithium silicate glasses can be obtained only with the mixtures containing of more than 70 mol% of SiO_2. In order to suppress devitrification, in this study lead oxide was added to the lithium silicate glasses. In the glass systems,lead oxide participates both as a network-forming oxide and as a glass network modifier. Among various forms of lead oxide, red lead (Pb_3O_4) is an interesting heavy metal oxide. Its presence in the glass composition can cause anincrease in the density and therefore an increase inthe refractive index to a greater extent. As a result, the scope of applications of the lithium silicate glasses widens. In fact, such materials find their application in non-linear optical devices in addition to their well-known application as electrolytes in solid state batteries. Strictly speaking, Pb_3O_4 decomposes at about 600 °C to PbO according to the following chemical equation: $2Pb_3O_4 \rightarrow 6PbO + O_2\uparrow$. During this reaction, PbO evolves from Pb_3O_4 through two intermediate polymorphs,α-PbO_2 and β-PbO_2. Among these two, the α-PbO_2 is a relatively less stable form, whereas β-PbO_2 is relatively

stable and exhibits good corrosion resistance even in acidic media [8,9]. The most important application of this oxide is as a cathode in the lead acid batteries [10]. However, by capturing $2e^{-}$, the PbO_2 converts in to PbO as per the reaction shown above. The lead ions in PbO_2 occupy mainly network forming positions with PbO_4 structural units which alternate SiO_4 structural units, whereas Pb^{2+} ions mainly act as glassmodifiers and also occupy network forming positions in PbO_4 units [11,12].

As per the crystallographic studies, the coordination geometries of lead complexes are of two categories. One of them is holodirected. In this, the lead ligand bonds are distributed throughout the surface of an encompassing globe and are nearly tetrahedral structures. According to Cambridge Structural Database all lead (IV) structures have a holodirected coordination geometry [13]. On the other hand, lead (II) structures are hemidirected for low coordination number (2-5), in which the lead–ligand bonds are directed throughout only part of an encompassing globe, viz., there is an identifiable void in the distribution of bonds to the ligands such as pyramidal structures.

Lead(II) with electron configuration [Xe] $4f^{14}5d^{10}6s^2$ is one of the post-transition metal elements that exhibits the so-called ‘‘inert-pair effect” [13, 14] which means the resistance of the pair of outer electrons on Pb(II) to removal or to participation in covalent bond formation. It has been explained as a relativistic effect causing the 6s orbital to contract, thereby increasing the energy required to remove or interact with the 6s lone pair of electrons. On the other hand, the *d* and *f* orbitals are destabilized because they expand radially as a result of screening from nuclear attraction by the s and p electrons. The result is a stable, relatively inert outer lone pair of electrons in case of Pb^{2+} ions [13, 14]

Altogether, by virtue of different valence states of lead ions in Pb_3O_4, it has a strong bearing on the diffusion of Ag^{+} ions and Li^{+} ions that are responsible for conductivity in the studied glass matrix.

Among various noble metal oxides, Ag_2O dissolves easily in the amorphous matrices. During the melting of the glasses with small concentration of Ag_2O,this oxide decomposes into Ag^0 (silver metallic particles) and Ag^+ ions at about 420 K [15].In general, the glasses consisting of noble metallic particles like silver particles, exhibit surface plasmon resonance (SPR) with the interaction of *E*-vector of the incident electromagnetic (e.m.) waves. TheSPR induces high local *E*- field in the neighbourhood of Ag ions [16] and hasstrong bearing on the electrical properties of the glasses to a great degree.

Further, the addition of small concentration of Ag_2O to lithium silicate glasses makes them a super ionic conducting glass. In fact, several recent studies on electrical properties of glasses containing noble metallic particles are available in the literature [17-19]. Moreover, such materials exhibit photo-catalytic activity with oxidation stability [20]. In general, in such materials, Ag ions, and electrons (e^-s) combinedly contribute to the conductivity. For this reason, the glasses containing Ag_2O are being used as important materials for electrodes and as electrolytes in chemical cells [21]. Overall, the conductivity of these glasses is projected (i) due to polaronic hopping between Ag ions of multiple valence states and in between Pb^{2+} and Pb^{4+}ions and (ii)due to the transport of silver and lithium ions.

The content of this study includes:(i) the methods of synthesis of Li_2O-Pb_3O_4-SiO_2 glasses doped with minor quantities (0 to 0.4 mol%) of Ag_2O, (ii) characterization of the glasses by means of X-ray diffraction (XRD), scanning electron microscopy (SEM), X-ray photoelectron spectroscopy (XPS) and differential thermal analysis (DTA) techniques, (iii) structural analysis of the prepared glasses as a function of Ag_2O content using IR and optical absorption spectra, (iv) detailed investigationson dielectric parameters viz., permittivity, loss tangent, electric moduli, dipolar relaxation effects, impedance diagrams and σ_a over a range of ω viz., 10^{-2} to 10^6 Hz and in the region of temperature 30 to 250°C and (v)

analysis of these results to have an understanding over the electrical conduction process as a function of structural changes occurring in the glass matrix due to variations in Ag_2O content.

2. Experimental

Different glasses (in mol %) in $(40\text{-}x)Li_2O\text{-}10Pb_3O_4\text{-}50SiO_2{:}xAg_2O$ series (with x = 0, 0.1, 0.2, 0.3 and 0.4) were prepared by general melt quenching technique. Based on the quantity of Ag_2O the glasses were designated as A_0, A_1, A_2, A_3 and A_4, respectively.The appropriate amounts of reagent grade chemicals were taken in platinum crucibles and were melted at 1400 ºC for 30 min. The resultant melt was then poured into brass moulds and subsequently annealed at 350 ºC so as to avoid internal bubbles, cracks, etc. To ensure the entrenchment of silver particles in the samples, they were heat treated at 250 °C for about 4 h and were chilled to room temperature. Later, the samples were finely ground and optically polished. The final dimensions of the samples used for the dielectric measurements wereapproximately 1.0 cm x 1.0 cm x 0.1 cm. A Carl Zeiss – EvoMA15A scanning electron microscopewas used to record the SEM images of the samples. Chemical make-up of the glasses was evaluated by energydispersive spectra (EDS) recorded with an Oxford-INCA Penta FETX3. XRD patterns of these samples were recorded on A RIGAKU-D/Maxb ULTIMA III X-ray diffractometer in the range of 2θ from 15° to 65°in the steps of 0.02 °/s with a scan speed of 2 deg/min.

The thermal behaviour of glasses was investigated by differential thermal analysis (DTA) using Mettler TGA/DSC 3+ thermo balance. Measurements were performed on powder samples (cca 40 mg) placed in an open Pt crucible and heated in an oxygen atmosphere from 25 up to 1000 °C at a rate of 20 °C min^{-1}. The results were analysed by applying the Mettler STARe 9.01 software and the glass transition temperature, T_g, was determined for each analysed sample.XPS studies were performed on PHI 5000 Versa Probe ULVAC instrument with Al Kα (1486.6 eV) as the source of X-rays. Electron emission angle

was45°. The stage the sample was kept on double sided carbon tape (in gifu) and the entire stage was placed into main entry chamber and kept for 12h. Etching of the samples was done with Ar^+ energy of 1kV for about 300 sec. 10^{-7} Pascal was the base pressure maintained. XPS were registered with C 1s peak at 284.6 eV as the reference.

The Fourier transform-infrared (FT-IR) spectra of the samples were recorded to a resolution of 0.1 cm^{-1}on a pre-calibrated (with a diamond crystal)Shimadzu IR TRACER 100 spectrophotometer in attenuated total reflectance (ATR)mode.A JASCO UV-VIS-NIR spectrophotometer was used to record optical absorption (OA) spectra of the samples to a precision of 0.1 nm in the wavelength region200–2000 nm.

For measuring dielectric properties, thin gold electrodes of nearly 0.6 cm in diameter, were sputtered on both sides of the glasses withSC7620 sputter coater. The dielectric and a.c. conductivity measurements were carried out on Novocontrol Alpha-AN Dielectric Spectrometer in the range of frequency 0.01 Hz- 1 MHz and in the range of temperature 30 - 250 °C (up to a precession of ±0.2°C). Equivalent circuits modelling and CNLLSQ(Complex Nonlinear Least Squares fitting) process was adoptedfor analysing the complex impedance diagrams.

3. Results and Discussion

Table 1 summarizes the concentration of Ag^+ ions and their average distance in the glass samples evaluated using the measured values of density and the average molecular weight.

Images ofLi$_2$O-Pb$_3$O$_4$-SiO$_2$ glasses containing varied amounts of Ag$_2$O were presented in Fig. 1. The samples with low concentrations of Ag$_2$O were found to be colourless and appeared to be light-yellow to brownish-yellow in colour as the Ag$_2$O content was increased. This demonstrated formation of forming colloidal Ag^0 particles (formed by

reducing Ag^{+} ions) and suggested larger concentration of Ag nanoparticles (Ag NPs) in the samples containing relatively larger concentration of silver oxide [22].

SEM images of post-heated glasses with varied contents of Ag_2O were shown in Fig. 2 which indicated the presence of well-defined unevenly dispersed crystallites (with a few μm size) embedded in the remnant glass phase. As the content of Ag_2O was increased, an increasing fraction of crystal grains with growing coalescence was observed. The chemical composition of the glasses was verified by EDS; the spectra suggested intact of all the expected elements in these glasses. Such a spectrum for the A_4 glass was shown in Fig. 2,

X-ray diffractograms (Fig.3) of the heat-treatedglasses showed peaks corresponding to Ag_2O (JPCDS 19-1155),AgO (JPCDS 43-1038) crystalline phases and Ag^0 (JPCDS 04-0783) particles [23-25]. Among these, Ag_2O is a cubic phase, whereas AgO is a monoclinic ($a = 5.85$, $b = 3.47$, $c = 5.49$, $\beta = 107.5^{o}$with space group $P2_1/c$) as shown in this figure [26]. With an increase in the Ag_2Ocontent, a gradual growth of the diffraction peaks related to Ag^0 particles was observed. These observations suggested a growing concentration of Ag^0 particles in the heat-treated samples.

DTAtraces of the investigated glasses were shown in Fig. 4. The traces exhibited a comparatively weak endothermic effect due to glass transition in the temperature range 400–415^{o}C. The thermograms exhibited multiple-exothermic peaks due to crystallization in the temperature range 500-700 ^{o}C with a prominent peak in the temperature region 500-600 °C.Another significant endothermic change due to re-melting of the sampleswas observed at about 900 °C.A brief summary of the results thermal analysis of these samples was given in Table 2. The results of differential thermal analysis suggested that the heat-treated samples comprised of multiple crystal phases. Further, a decrease in T_{c1}-$T_g$was observed with increase in Ag_2O content (Table 2).The observed decrease suggested an increased degree of de-vitrification of the glass samples.

Fig. 5,shows XPS spectrum of the glass A_2. The deconvoluted and fitted spectrum exhibited three peaks at 137.5 eV,137.9eV and 138.4eV corresponding to PbO_2,PbO and Pb_3O_4 region of $Pb4f_{7/2}$. Three other peaks at 142.36eV, 142.76 eV and 143.26 eV corresponding to PbO_2, PbO and Pb_3O_4 region of $Pb4f_{5/2}$were also observed in this spectrum [27]. With anincrease inAg_2O concentration, the peak corresponding to PbO_2 exhibited a gradual growth at the expense of Pb_3O_4 peak (inset of Fig. 5). This observation suggested that there was a gradual growth of $Pb^{(IV)}$-O bondings in the glass network that facilitated the increased degree of structural augmentation. Such augmentation was predicted to be a hindrance for the easy transport of charge carriers that contribute to the conductivity

XPS spectrum of the glass A_2 recorded in the energy region of Ag 3dwas presented in Fig. 6. The spectrum showed the peaks at 367.2 and 373.1eV, respectively, associated with Ag^+ (Ag $3d_{3/2}$) and Ag^0 (Ag $3d_{5/2}$) NPS [28]. A feeble kink corresponding to Ag^{2+} ions was also observed in this spectrum at 367.5 eV [28, 29]. In the inset of this diagram variations of the intensities of the peaks corresponding to Ag^+ ions and Ag^0 metallic particles were plotted against concentration of Ag_2O. The inset showed the gradual growth of the peak corresponding to Ag^0 metallic particles, whereas the peak related to Ag^+ ions that contribute to the ionic conductivity gradually decreased.

The optical absorption spectra of Li_2O–Pb_2O_3-SiO_2: Ag_2O glass recorded in the wavelength region 250-800 nm were presented in Fig.7.Pure glass (A_0) exhibited cut-off wavelength at 330.5 nm. With the gradual increase in Ag_2O from 0.1 to 0.4 mol%, the edge exhibited spectrally blue shift. Moreover, these spectra exhibited an absorption band in the spectral region 340– 460 nm. In general Ag^+ ions get transformed to metastable$Ag^0(4d^{10}5s^1)$ metallic particles [30]. These unstable Ag^0 particles interact with Ag^+ ions and Ag^+-Ag^0 clusters form in the material. There occurs surface plasmon resonance (SPR) between the coherent oscillations of e^-s on the top of Ag^+-Ag^0 groups and the e.m. waves incident upon

the material. The visualised peak in the spectra represented such resonance [31]. Further, this band exhibited a growth with Ag_2O content.It indicated increasing presence of Ag^0 particles with the rise of Ag_2O content in the glasses. Additionally, the SPR band exhibited red shift with the concentration of Ag_2O.. Some of for reasons for that red shift include the increasing dimensions of the clusters of silver particles, scattering contribution to SPR band and there may be changein the absorption from dipoles to multipoles etc. [32-34].

To estimate the optical band gap (E_o) and to study its dependence on Ag_2O concentration, Tauc plots ($(\alpha\hbar\omega)^{1/2}$ *vs* $\hbar\omega$) weredrawn in Fig. 8. The value of E_o(evaluated from the extrapolation of the curves to the X -axis) exhibited an increasing trend with Ag_2O concentration (Table 3). XPS results indicated that there was an increase in Pb^{4+} ion concentration with an increase in Ag_2O content. Tetravalent lead ions take part in glass network forming positions through Pb^{IV}-O-Si^{IV} linkages. Such interconnectivity among various structural groups caused a decrease in the degree of localization of free e^-s and decreased the concentration of donor centres and lead to enlarged E_o.

Yet, a variation in E_o with Ag_2O content is connected with the interactions of *p*-e^-s of Pb and *d*- e^-s of Ag ions. XPS and even XRD results revealed an increase in Ag^+ ions' concentration which were reduced to Ag^0 particles. This caused a decrease in the donor centres' concentration. For this reason, the electrons trapped at energy states of Ag^+ions get distanced to a larger degree with the empty 4*d* energy levels of Ag^0 particles. As a result, width of the band constitutes energy levels of Ag^0 impurity contracted in the band gap of the host glass and caused to enlarge E_o with the increase of Ag_2O content.

Shifting of SPR band towards longer wavelength with increased Ag_2O content (Table 3) indicated mutual exchange of polarons amongAg^0-Ag^+ pairs [35]. Effective radial wave-function of e^-s trapped at less deeper traps in the band gap was shorter because of insignificant local oscillations of potentials compared to transfer integral *j*. As a result, the

magnitude of superposition of wavefunctions of the electrons in the closely spaced sites reduced and facilitated the creation of polaron. In summary, the resultsof optical absorption of Ag_2O doped Li_2O-Pb_3O_4-SiO_2 glasses suggested the possible polaronic transfer between Ag^0-Ag^+ pairs. Such type of transfer predicted to be vital for analysing the dielectric results [36].

The IR spectra of the studied glasses (Fig. 9) exhibited two prominent bands ascribed toasymmetric and symmetric stretching vibrations O–Si–O ofSiO_4 units at about 1012 cm^{-1} and at 790 cm^{-1}, respectively [37]. Additionally, the spectra also exhibited two vibrational bands at 578 cm^{-1}(identified as the characteristic vibrations of $Pb^{(IV)}$-O bond of PbO_4 units[8]) and at 460 cm^{-1} (conventional band due to $Pb^{(II)}$-O vibrations [37]). With the gradual increase of Ag_2O concentration, the bands due to symmetrical vibrations of O–Si–O groups and also those of PbO_4 structural groups were observed to grow. Such growth indicated a growing degree of structural augmentation. Positions of different vibrational bands visualized in these spectra were summarized in Table 4.

Variation of dielectric constant $\varepsilon'(\omega)$with ω at different temperatures (for two of the glasses *viz.*, A_1 and A_2 were shown in Fig. 10 (a) and with T at various ω (for A_3 and A_4 glasses) were shown in Fig. 10 (b). With the increase in ω,$\varepsilon'(\omega)$ exhibited a decreasing trend and a high frequency plateau value $\varepsilon'_\infty(\omega)$ was reached. With temperature, $\varepsilon'(\omega)$ exhibited a larger dispersion at high T and larger values at low frequencies (increased from 10^2 to 10^5 with increase of temperature from 30 to 250 °C). Among different electrical polarizations, the space charge polarization (piling up of charge carriers at the electrodes) caused to increase thevalue of $\varepsilon'(\omega)$at lower frequencies. In general, the quantum of this polarization is dependent on long range diffusion (which depends on the degree of structural defragmentation) of free charge carriers). To put it differently, the largerincrease of f $\varepsilon'(\omega)$ at low ω region was because of easy diffusion of conducting species in the material. In high ω

region, the oscillation frequency of the conducting species was relatively lower. For this reason, $\varepsilon'(\omega)$reached high frequency plateau$\varepsilon'_{\infty}(\omega)$ as shown in Fig.10(a).

In the inset of Fig.10(a),the dependence of $\varepsilon'(\omega)$on the concentration of Ag_2O(at a fixed ω and T) was plotted. $\varepsilon'(\omega)$ showed a descending tendency with the increase of Ag_2O concentration.XPS and IR spectral studies suggested increased proportion of Pb^{4+} ions which occupy tetrahedral positions in this glass network and cross-link with SiO_4units. Such cross-linkages obstructed the passage of charge carriers towards electrodes [38, 39] and decreased the value of dielectric constant.

Variations of loss tangent (tan δ) with frequency and temperature for the sample A_4 were presented in Fig. 11. Thevariations indicated dipolar relaxation behaviourmore clearly in the low ω range. Nevertheless, in the high ω region the dipolar effects were not distinct; electrode phenomenon appeared to be dominating over the inherent dipolar effects in thisfrequency range. Hence, to throw more light on the inherent dipolar effects, electric moduli formulation was adopted. According to this formalism, electric modulus M*, is given by

$$M^* = M' + iM'', \qquad (1)$$

$$\text{Where, } M' = \frac{\varepsilon'(\omega)}{(\varepsilon'(\omega))^2 + (\varepsilon''(\omega))^2} \qquad (2)$$

$$\text{And } M'' = \frac{\varepsilon''(\omega)}{(\varepsilon'(\omega))^2 + (\varepsilon''(\omega))^2}; \qquad (3)$$

Using the values of $\varepsilon'(\omega)$ and $\varepsilon''(\omega)$, M' and M'' were evaluated and their variations with ω and Twere presented Fig. 12. A clear dipolar relaxation character of the inherent dipoles could be visualized from these plots.

Using the resonant frequency ω_r (points of intersection of M' and M''), the relaxation time τ was determined and its variation with T was plotted in Fig. 13 for all the samples. The variation showed a decreasing tendency with T and found to be independent of temperature

at highertemperatures. Variation of τ with Ag_2O content at a fixed T was observed to increase (Table 5). From the plots of $\ln\tau$ vs$1/T$, the activation energy W_d for dipoles was estimated using the equation $\tau = \tau_0 \exp(W_d/k_BT)$ and presented in Table5. W_d exhibited an increase with the increase in the concentration of Ag_2O. Such increase of W_d and also τ with the content of Ag_2O suggested decreased magnitude of freedom for dipoles to orient in the field direction.

To shed additional light on dipolar effects of the samples, Cole-Cole diagrams between M'' *vs* M' at higher temperatures were drawn and presented in Fig. 14 for the glass samples A_3 and A_4. The plots were observed to be semi-circular arcs with centers lying below the X-axis. The obtained values of angle (α') between line connecting the center of arc and the X-axis at the origin are presented in Table5. $\alpha'$was found to decrease with increase of Ag_2O content and suggesteddecreasing degree of distribution of τ. In general, spreading of relaxation times is due to multiple types of dipoles with various dipole moments [40]. Additionally, entrenchment of dipoles in asymmetrical potential regions also accounts for such spreading[7]. The decreased value of α' suggested the decreasing asymmetric environment for the dipoles as was also suggested by IR spectral studies. The complexes of divalent silver ions and also divalent lead ions did contribute for dipolar relaxation effects. The growing concentration of tetravalent lead ions that occupy the glass network forming positions resist the freedom for dipoles to oscillate and increased activation energy for dipoles.

Figs. 15(a) and (b), respectively, represent the variations of real (Z') and imaginary (Z'') parts of impedancewith frequency at different temperatures for the glass A_2. Out of the two components of impedance, the real component Z' (a pure resistance component) showed a decrease with ω (even though it exhibited a minor non-linearity in the low ω range, (likely due to electrode effect). The imaginary part Z″, however, showed large spreading with Tin

the low frequency region (< 1 kHz). Moreover, nearly up to 1 kHz, this component exhibited a linear increase with ω especially at higher temperatures. This type of behaviour indicated inductive reactance component ($L\omega$). However, at higher frequencies (beyond 1kHz) the Z'' component with frequency exhibited an inverse proportionality. Such behaviour is acharacteristic of capacitive reactance (*viz*., $1/C\omega$). Tothrow more light on the physical significance of these diagrams, in Fig. 15(c), Z'' and M'' *vs* frequency at 200°C were plotted forA_2sample. The peaks of these two quantities were found to be slightly deviated and suggested that long-range interaction was the main reason for such a confined relaxation character of these glasses [41].

To know the dependence of magnitude of the impedance of Li_2O-Pb_3O_4-SiO_2:Ag_2O glass samples on the content of Ag_2O, impedance plots (or Nyquist plots) between Z'' *vs* Z' were drawn. Figs. 16 (a), (b) and (c) represented such plots for the sample A_2 drawn in different temperature regions. Area enclosed by the curve exhibited a decrease with temperature and indicated a decrease in the impedance of the samples with temperature. The comparison of impedance plots for all the samples drawn at 250 °C was shown in Fig. 16(d) along with the equivalent circuit diagram The area under the curves was observed to increasewith increase of Ag_2O content and suggested an increase of *Z.* Moreover, the diagrams exhibited semi-circular shape withinclined spur (at low ω and high *T* regions) due to thermally stimulated mobility of the conducting species.

These diagrams further indicated two kinds of conducting species in the glass samples. Semi-circular arc associated with bulk conduction and the inclined spur represented the piling of charge carriers on surface electrodes of the glasses. Larger magnitude of such spur, suggested larger concentration of conducting species that accumulated at the electrodes. In this investigation, a descending size of magnitude of this spur along with growth of the area enclosed by the semicircle was observed with the increase of Ag_2O concentration. This

behaviourindicated increasing magnitude of the resistance for the migration of Li^+ and Ag^+ions (conducting ions) towards the electrodes. The impedance behaviour was analysed further, by Bode plots (impedance $|Z|$ and $\tan\varphi = Z''/Z'$ *vs* ω). Such diagram for a particular glass A_4drawn at 200 °C was presented in Fig. 16(e). The graph suggested that $|Z|$ was higher at low ω region and lower in the high ω region and indicated that electronic/polaronic (or Faradic) current was responsible for the impedance [42, 43].

In Figs.17 (a)and 17 (b),$\ln\sigma_{ac}$ (ac conductivity) was plotted against ω and against $1/T$ for the glass A_4, respectively. In the high T region and in the low ω range($\sigma_{ac}(\omega)\rightarrow\sigma_{dc}$)the plots were found to be near frequency independent; it was observed to be near temperature invariant on T in the high ω and low temperature regions and it varied linearly with ω viz., $\sigma_{ac}(\omega) \propto \omega$. The general relationship between $\sigma_{ac}(\omega)$ and ω however, seemed to be $\sigma_{ac}(\omega) \propto \omega^s$, where s=1 in the high ω and low$T$ regions; the ωexponent s is the universal dielectric response (UDR) exponent; normally, s<1.

In the intermediate ω region, a '*to* and *fro*' hopping of conducting species (polarons in this case) occurred due coulombic repulsion. Structural investigations suggested that Pb and Ag ions existed in multiple valence states. Hence, the polaronic exchange between $Pb^{2+}$and Pb^{4+} andAg^0 to Ag^+ ions took place and contributed to the σ_{ac} in addition to the ionic contribution from Li^+ and Ag^+ ions. In the inset of Fig. 17 (a) the dependence of σ_{ac} (measured at 1 kHz and 250 °C) on the concentration of Ag_2O was plotted. The plot suggested a gradual decrease of σ_{ac} with Ag_2O content. The obtained vales of σ_{ac} were found to be comparable with that of various other glass systems containing Ag_2O (Table 6)[28, 44-47]

From the plots of $\ln\sigma_{ac}$ vs$1/T$, the activation energy W_{ac} was evaluated and itwas found to increase with increase of Ag_2Oconcentration (Table 5). Such increment suggested a

decreasing magnitude of free volume space available for easy movement of conducting species in the glasses with increase of Ag_2O content.

UDR exponent *s* was estimated from the plots of log $\sigma_{ac}(\omega)$ vs log ω (drawn in the intermediateω region). Such plot was presented in Fig. 18 for the glass A_4. The value of *s*showed a decreasing trend with *T* (inset of Fig. 18). The decrease of the exponent suggested that conduction consists of polaronic tunneling[44]. Variation of *s* with Ag_2Ocontent indicated anincreasing trend (Table 5). Such increase indicated a decrease in the magnitude of free space available for the diffusion of Li^+ and Ag^+ ions with increase of Ag_2O content [48]. From the analysis of the results of structural studies, we found that in the samples containing larger concentration Ag_2O, there was a lager concentration of Pb^{IV}-O units that cross link with SiO_4 units. Such cross linkages obstruct the easy transport of conducting species like Li^+ and Ag^+ ions. As a result, a decrement in the conductivity was observed.

Further, a near invariance of $\sigma_{ac}$with*T*in the low *T* region especially in the high frequency range (Fig. 17(b)) was observed. Such behavior of conductivity was analyzed using quantum mechanical tunneling (QMT) model [49]. As per this model this model,the density of defect energy states $N(E_F)$ was evaluatedusing the expression

$$N(E_F) = \left[\frac{3\sigma(\omega)}{\pi e^2 k_B T(\alpha'')^{-5}\omega\left[ln\frac{\nu_{ph}}{\omega}\right]^4}\right]^{1/2} \qquad (4)$$

In Eq. (4), α" is the electronic wave function decay constant (evaluated to be ~ 0.45(Å)$^{-1}$ by plotting log σ_{ac}vs R_i, inter-ionic separation of Ag ions), ν_{ph} is phonon frequency, *e* is the electron charge. Value of $N(E_F)$evaluated (at 1 kHz and at 473 K) showed a decreasing trend with Ag_2O concentration (Table 5). This result further confirmed that there was a decreasing concentration of defects in the glass (that caused to lower the σ_{ac}) with increase of Ag_2O concentration.

4 Conclusions

Li_2O-Pb_3O_4-SiO_2:Ag_2O glasses were synthesized. The results of characterization suggested that the glasses were composed of Ag^+, Ag^{2+}, Pb^{4+}, Pb^{2+} ions and Ag^0 metallic particles. The results further suggested an increase in the concentration of tetrahedral Pb^{4+} ions which cross-link with SiO_4 units. The observed decrease in the dielectric permittivity with Ag_2O concentration was attributed to the decreased magnitude of scp because of decreased concentration of free volume imperfections. The observed dipolar relaxation effects were analysed using Cole-Cole diagrams. Ac conductivity (σ_{ac}) was ascribed to the polaronic transfer between multiple valence states of Ag ions and also Pb ions in addition to the diffusion of Li^+ and Ag^+ ions. The observed decrease of σ_{ac} with Ag_2O content was attributed to the increased degree of polymerization of the glass network. Overall, it appeared the presence of red lead was an obstruction for the conductivity even in fast ion conducting glasses.

Credit author statement

T.V.N. Keertikut: Conceptualization, Methodology, Investigation. **Sara Marijan**: Data curation, Formal analysis, Software, Writing – original draft. **Jana Pisk**: Methodology, Data curation, Formal analysis, Software, Writing – original draft. **A. VenkataSekhar**: Methodology, Data curation, Formal analysis. **A. Siva Sesha Reddy**: Methodology, Data curation, Formal analysis. **N. Venkatramaiah**: Methodology, Data curation, Formal analysis. **G. Naga Raju**: Conceptualization, Methodology, Data curation, Investigation. **L. Pavić:** Data curation, Formal analysis, Software, Writing – original draft. and**N. Veeraiah**: Supervision, Writing – original draft, Writing – review & editing.

Acknowledgement

J.P. acknowledges the support of project CIuK co-financed by the Croatian Government and the European Union through the European Regional Development Fund-Competitiveness and Cohesion Operational Programme (Grant KK.01.1.1.02.0016.).

References

[1] C. Devaraja, G. V. Jagadeesha Gowda, B. Eraiah, Asha M. Talwar, A. Dahshan, S.N. Nazrin, Structural, conductivity and dielectric properties of europium trioxide doped lead boro-tellurite glasses, J. Alloys Compd. 898 (2022) 162967.

[2] Mohammed A. Algradee, Y.H. Elbashar, A.B. Alwany, H.H. Hassan, R. El-Mallawany, Impact of Yb_2O_3 on the physical, bonding, dispersion and dielectric properties of $Li_2O–ZnO–P_2O_5$ glasses, Mater. Sci. Semicond. Process. 140 (2022) 106362.

[3] X. Shao, Y. Hu, Y. Zhao, S. Chen, L. Liu, J. Chen, J. Li, Crystallization and dielectric properties of oxyfluoridealuminosilicate glasses added with Na_2O, J. Non-Cryst. Solids 576 (2022) 121261.

[4] J. Li, J. Huang, H. Feng, X. Wang, X. Yin Y. Zhang, Effect of TiO_2/SiO_2 molar ratio on the structure, dielectric and crystallization properties of SiO_2-TiO_2-ZrO_2-RO-Al_2O_3 glasses, J. Non-Cryst. Solids 576 (2022) 121243.

[5] Q. Chen, Z. Li, H. Wang, Influence of polarization, multi-valences and multi-coordination of cobalt: Third-order nonlinear, dielectric and Faraday properties of Bi0.5Co1.5S3/high optical basicity glass, Mater. Res. Bull. 145 (2022) 111531.

[6] G. El-Damrawi, A.M. Abdelghany, M.A. Madshal, AC conductivity and dielectric properties of Cr_2O_3 doped $SrO–P_2O_5$glasses, Physica B 618 (2021) 413184.

[7] S. R. Elliott. Physics of amorphous materials, Longman, London,1990.

[8] D. Guo, C. Robinson, J.E. Herrera, Mechanism of dissolution of minium (Pb3O4) in water under depleting chlorine conditions, Corrosion Science 103 (2016) 42–49

[9] H. Zhang, S.H. Liu, F. Liu, S.L. Yan, W.Y. Li, Study on the reaction mechanism between Pb_3O_4 and Si in stored silicon delay composition, J. Thermal Analysis Calorim. 132 (2018):327–336.

[10] Greenwood, N. Norman; Earnshaw, Alan (1997). Chemistry of the Elements (2nd ed.). Butterworth-Heinemann. p. 386. ISBN 978-0-08-037941-8

[11] A. Siva Sesha Reddy, G. Lakshminarayana, N. Purnachand, V.R. Kumar, N. Venkatramaiah, V. Ravi Kumar, N. Veeraiah, Influence of gold ions on visible and NIR luminescence features of Er3+ ions in lead boroselenate glass ceramics, J. Lumin. 226 (2020) 117481.

[12] A. Subba Rao, I.V. Kityk, J. Ashok, V. Ravi Kumar K.J. Plucinski, A. Siva Sesha Reddy, K. Naresh Kumar, N. Veeraiah, Physical characteristics of $PbO–ZrO_2–SiO_2$:TiO_2 glass ceramics embedded with $Pb_2Ti_2O_6$ cubic pyrochlore crystal phase: Part-II piezo-optical acoustic and elastic Properties, J. Alloys Compd. 725 (2017) 318-325.

[13] Liat Shimoni-Livny, Jenny P. Glusker, Charles W. Bock , Lone pair functionality in divalent lead compounds, Inorg. Chem., 37 (1998)1853-1867

[14] Martin Breza, Lukáš Bucˇinsky´ , Stanislava Šoralová, Stanislav Biskupic, On the origin of the hemidirected geometry of tetracoordinated lead (II) compounds, Chemical Physics 368 (2010) 14–19.

[15] S. Rada, M. Rada, R.V. Erhan, V. Bodnarchuk, L. Barbu-Tudoran, E. Culea, Heterogeneities in the silver oxide-lead-germanate glasses, J. Alloys Compd. 770 (2019) 395-404.

[16] N. Chakchouk, B. Louati, K. Guidara, Ionic conductivity and dielectric relaxation studies of a low-temperature form of silver zinc phosphate, J. Alloys Compd. 747 (2018) 543-549.

[17] D. Chen, X. Qiao, X. Qiu, J. Chen, Synthesis and electrical properties of uniform silver nanoparticles for electronic applications, Journal of Materials Science 44 (2009) 1076-1081.

[18] A Kumar , N Mehta , A. Dahshan, A new approach for nano-structuring of glassy selenium (g-Se) using silver nanoparticles (AgNPs) as precursor, Mater. Today Commun. 26 (2021) 101719.

[19] D.K. Božanić, R. Dojčilović, J.D. Pajović, D. Tošić, D. Dudić, M. Réfrégiers, V. Djoković, Fluorescence microscopy and photodielectric characterization studies of the composite films of polyvinyl alcohol and tryptophan functionalized silver nanoparticles, Colloids Surf. A: Physicochem. Eng. Asp. 634 (2022) 128050.

[20] K. Sklepic, M. Vorokhta, P. Mosner, L. Koudelka, A. Mogus-Milankovic, Electrical mobility of silver ion in Ag2O-B2O3-P2O5-TeO2 glasses, J. Phys. Chem. B 118 (2014) 12050e12058.

[21] M. Nagarjuna, T. Satyanarayana, Y. Gandhi, N. Veeraiah, Influence of Ag_2O on some physical properties of LiF-TiO_2-P_2O_5 glass system, J. Alloy. Comp. 479 (2009) 549-556.

[22] H. Fares, T. Castro, J.R. Orives, D.F. Franco, M. Nalin, White light and multicolor emission tuning in Ag nanocluster doped fluorophosphate glasses, RSC Adv. 7 (2017) 44356-44365.

[23] S.S. Kabalkina, S.V. Popova, N.R. Serebryanaya, L.F. Vereshchagin, A New modification of Ag2O with a layer structure, Sov. Phys. Dokl. 8 (1964) 972.

[24] D. Grier, G. McCarthy, JCPDS-international Centre for Diffraction Data, USA, 1997.

[25] M. Bosca, L. Pop, G. Borodi, P. Pascuta, E. Culea, XRD and FTIR structural investigations of erbium-doped bismuth-lead-silver glasses and glass ceramics, J. Alloy. Comp. 479 (2009) 579-582.

[26] L. Savio, C. Giallombardo, L. Vattuone, A. Kokalj, M. Rocca, Tuning thestoichiometry of surface oxide phases by step morphology: Ag (511) versus Ag(210), Phys. Rev. Lett. 101 (2008) 266103-266104.

[27] Y. He, R. Xu, S. He, H. Chen, K. Li, Y. Zhu, Q. Shen, An investigation of the NO3- concentration effect on lead anodic electrochemical behavior in NaOH solution, Int. J. Electrochem. Sci., 12 (2017) 9697 – 9713.

[28] V. Prasad, L. Pavic, A. Mogus-Milankovic, A. Siva Sesha Reddy, Y. Gandhi, V. Ravi Kumar, G. Naga Raju, N. Veeraiah, Influence of silver ion concentration on dielectric characteristics of Li_2O-Nb_2O_5-P_2O_5 glasses, J. Alloy. Comp. 773 (2019) 654-665.

[29] W. Wei, X. Mao, L.A. Ortiz, D.R. Sadoway, Oriented silver oxide nanostructures synthesized through a template-free electrochemical route, J. Mater. Chem. 21 (2011) 432-438.

[30] V.M. Renteria, J. Garcia-Macedo, Modeling of optical absorption of silver prolate nanoparticles stabilized by Gemini surfactant, Colloids Surf. A 273 (2006) 1-3.

[31] K. Naresh Kumar, M. Kostrzewa, Ingram Adam, B. Suresh, A. Siva Sesha Reddy, Y. Gandhi, M. Piasecki, N. Veeraiah, Dielectric features, relaxation dynamics and a.c. conductivity studies on Agþ mixed lead arsenate glass ceramics, J. Mater. Sci. Mater. Electron. 29 (2018) 1153-1172.

[32] Q.Z. Zhao, J.R. Qiu, X.W. Jiang, C.Z. Zhao, C.S. Zhu, Mechanisms of the refractive index change in femtosecond laser-irradiated Au^{3+} doped silicate glasses, J. Appl. Phys. 96 (2004) 122-7125.

[33] J.P. Juste, I.P. Santos, L.M.L. Marz_an, P. Mulvaney, Gold nanorods: synthesis characterization and applications, Coord. Chem. Rev. 249 (2005) 1870-1901.

[34] U. Kreibig, C.V. Fragstein, The limitation of electron mean free path in small silver particles, J. Phys. A 224 (1969) 307-323.

[35] T. Hayakawa, S. Tamil Selvan, M. Nogami, Field enhancement effect of small Ag particles on the fluorescence from Eu^{3+}-doped SiO_2 glass, Appl. Phys. Lett. 74 (1999) 1513-1515.

[36] B.V.R. Chowdari, P. PramodaKumari, Studies on Ag_2O, MxOy, TeO_2 (MxOy¼ WO_3, MoO_3, P_2O_5 and B_2O_3) ionic conducting glasses, Solid State Ionics 113 (1998) 665-675.

[37] K.J. Rao, Structural Chemistry of Glasses, Elsevier, Amsterdam, 2002.

[38] K. Srilatha, L. Pavic, A. Mogus-Milankovic, Ch. SrinivasaRao, G. Little Flower, V. Ravi Kumar, N. Veeraiah, The role of vanadium valence states and coordination on electrical conduction in lithium iodide borate glasses mixed with small concentration of silver iodide, J. Non-Cryst. Solids 357 (2011) 3538-3547.

[39] L.S. Rao, M.S. Reddy, D.K. Rao, N. Veeraiah, Influence of redox behavior of copper ions on dielectric and spectroscopic properties of Li_2O-MoO_3-B_2O_3:CuO glass system, Solid State Sci. 11 (2009) 578-587.

[40] C.J.F. Bottcher and P. Bordewijk, Theory of Electrical Polarization, Elsevier, Amsterdam, 1978.

[41] M. Coşkun, Ö. Polat, F.M. Coşkun, Z. Durmuş, M. Çağlar, A. Türüt, The electrical modulus and other dielectric properties by the impedance spectroscopy of $LaCrO_3$ and $LaCr_{0.90}Ir_{0.10}O_3$perovskites, RSC Adv. 8 (2018) 4634–4648.

[42] J. Ashok, N. Purnachand, J. Suresh Kumar, M. Srinivasa Reddy, B. Suresh, M.P.F. Graça, N. Veeraiah, Studies on dielectric dispersion, relaxation kinetics and a.c. conductivity of Na_2O−CuO−SiO_2 glasses mixed with different concentrations of Bi_2O_3-Influence of redox behaviour of copper ions, J. Alloys Compd. 696 (2017) 1260−1268.

[43] A. Moguš-Milanković, L. Pavić, K. Srilatha, Ch. SrinivasaRao, T. Srikumar, Y. Gandhi and N. Veeraiah, Electrical, dielectric and spectroscopic studies on MnO doped LiI-AgI-B_2O_3 glasses, J. Appl. Phys. 111 (2012) 013714.

[44] J. Ashok, M. Kostrzewa, A. Ingram, N. Venkatramaiah, M. Srinivasa Reddy, V. Ravi Kumar, M. Piasecki, N. Veeraiah, Structural and dielectric features of silver doped sodium antimonate glass ceramics, J. Alloys Compd. 791 (2019) 28-295.

[45] M. Nagarjuna, P. RaghavaRao, Y. Gandhi, V. Ravi kumar, N. Veeraiah, Electrical conduction and other related properties of silver ion doped LiF–V2O5–P2O5 glass system, Physica B 405 (2010) 668-677

[46] S. Bhattacharya, A. Ghosh, Conductivity relaxation in some fast ion-conducting AgI–Ag2O–V2O5 glasses, Solid State Ionics 161 (2003) 61-65

[47] Dipankar Biswas, R.K. Nanao, Ningthemcha, LoitongbamSurajkumar Singh, Rittwic kMondal, Soumyajyoti Kabi, AnindyaS undar Das, Effect of AgI doping on electrical conductivity and dielectric relaxation in silver phosphate glass nanocomposite systems, Physica B 602 (2021) 412486

[48] C. Filipicˇ, A. Moguˇs-Milankovic´, L. Pavic´, K. Srilatha, N. Veeraiah, Polaronicbehavior of MnO doped LiI-AgI-B_2O_3 glass, J. Appl. Phys. 112 (2012) 073705.

[49] G. Austin and N.F. Mott, Polarons in crystalline and non-crystalline materials, Adv. Phys. 50 (2001) 757.

Caption for Tables

Table 1 Details of composition (all in mol%) of the glass samples used.

Table 2 Summary of the data on differential thermogravimetric studies

Table 3 Summary of the data on optical absorption spectra of $Li_2O{-}Pb_3O_4{-}SiO_2{:}Ag_2O$ glasses. The band positions are measured to an accuracy of ±1 nm.

Table 4 Summary of the data of band positions (in cm^{-1}) of various structural units in FT–IR spectra of $Li_2O{-}Pb_3O_4{-}SiO_2{:}Ag_2O$glasses. The values of the peak positions are measured to precision of ±1 cm^{-1}.

Table 5 Summary of the data on a.c. conductivity and other parameters of Ag_2O doped$Li_2O{-}Pb_3O_4{-}SiO_2$ glasses.

Table 6 A.c. conductivity of various glass systems doped with Ag_2O measured at I kHz and 200 ºC)

Caption for Figures

Fig. 1 Photographs of the heat treated Li_2O-Pb_3O_4-SiO_2 glasses doped with different concentrations of Ag_2O.

Fig. 2 SEM images of heat treated Li_2O-Pb_3O_4-SiO_2 glasses doped with different concentrations of Ag_2O. The figure also consists of EDS for the sample A_4.

Fig. 3 XRD profiles of heat treated Li_2O-Pb_3O_4-SiO_2 glasses doped with different concentrations of Ag_2O.

Fig. 4 DTA traces of heat treated Li_2O-Pb_3O_4-SiO_2 glasses doped with different concentrations of Ag_2O.

Fig. 5 Deconvoluted and fitted XPS spectra of PbO, PbO_2 and Pb_3O_4 in the glass sampleA_2 and inset represents the intensity variation of PbO_2 and Pb_3O_4 ($4f_{7/2}$) with the concentration of silver oxide.

Fig. 6 Deconvoluted and fitted XPS spectra of Ag^0 and Ag^+ ions in the glass samples A_2 and the insets represents the intensity variation of Ag^0 and Ag^+ ions with the concentration of silver oxide.

Fig. 7 Optical absorption spectra of Li_2O-Pb_3O_4-SiO_2 glasses doped with different concentrations of Ag_2O recorded after heat treatment.

Fig. 8 Tauc plots of heat treated Li_2O-Pb_3O_4-SiO_2 glasses doped with different concentrations of Ag_2O.

Fig. 9 IR spectra of heat treated Li_2O-Pb_3O_4-SiO_2 glasses doped with different concentrations of Ag_2O.

Fig. 10 (a) Variations of dielectric constant with frequency measured at different temperatures for the sample A_1 and A_2.

Fig. 10 (b) Variations of dielectric constant with temperature measured at different frequencies for the sample A_3 and A_4.

Fig. 11 Variations of dielectric loss (a) with frequency measured at different temperatures and (b) with temperatures for the sample A_4

Fig. 12 Variations of electric moduli M′ and M″ (a) with frequency at different temperatures and (b) with temperature at different frequencies for the sample A_3

Fig. 13 The plots of relaxation times vs temperature for Li_2O-Pb_3O_4-SiO_2 glasses doped with different concentrations of Ag_2O.In this figure the variations of τ evalauted at 470 K with the concentration of Ag_2O is also presneted.

Fig. 14 Cole-Cole plots for the samples A_3 and A_4

Fig. 15 Variations of Z′ vs Z″ with frequency at different temperatures for the samples A_2

Fig. 15(c) Variation of M″ (ω) and Z″(ω) with frequency at 200 °C for the glass A_2.

Fig. 16 (a) The plots of Z′ vs Z″ drawn in the temperature regions (a) 30-50 °C (b) 100-150 °C (c) 225-250 °C for the sample A_4.

Fig. 16(d) The comparison plots of impedance of temperature of Li_2O-Pb_3O_4-SiO_2 glasses doped with different concentrations of Ag_2Odrawn at 250 °C. In the equivalent circuit diagram the parallel CR circuit accounts for semi-circular path of the diagram whereas additional series capacitor represents the inclined spur part.

Fig.16(e) Bode plots (plots of total impedance $|Z|$ and the phase angle, $\tan\varphi = Z''/Z'$ *vs* ω) for a selected glass sample A_4drawn at 200 °C

Fig. 17 The plots of σ_{ac} (a) vs frequency drawn at different temperatures and (b) vs 1/T drawn at different frequencies for the glass samples A_4. Inset represents the variation of σ_{ac} with concentration of Ag_2O measured at 250°C and 1 kHz.

Fig. 18 Plots of log $\sigma_{ac}(\omega)$ versus log ω for the glass sample A_2drawn at different temperatures and to evaluate frequency exponent*s*.

Table 1

Details of composition (all in mol%) of the glass samples used.

Glass	Conc. Ag_2O (mol%)	Density d (g/cm^3) (±0.001)	Silver ion conc. N_i(x10^{19} /cm^3) (±0.01)	Interionic distance of silver ions R_i (Å)(±0.01)	Polaron radius R_p(Å) (±0.01)
A_0	0	3.998	--	--	--
A_1	0.1	4.027	1.366	4.18	1.68
A_2	0.2	4.031	2.731	3.32	1.33
A_3	0.3	4.038	4.101	2.89	1.16
A_4	0.4	4.083	5.466	2.63	1.06

Table 2

Summary of the data on differential thermo gravimetric studies

Glass	Glass transition temperature T_g (±1 °C)	Crystallization temperature T_c (±1 °C)	T_c-T_g(±1 °C)
A_0	404	591	187
A_1	413	584	171
A_2	409	574	165
A_3	407	565	158
A_4	405	549	144

Table 3

Summary of the data on optical absorption spectra of $Li_2O–Pb_3O_4–SiO_2:Ag_2O$glasses. The band positions are measured to an accuracy of ±1 nm.

Absorption Band details → Glass ↓	A_0	A_1	A_2	A_3	A_4
SPR band position	--	406	409	411	419
Cut-off wavelength (nm)	330	312	300	291	276
Optical bandgap E_o (eV)	3.31	3.50	3.59	3.76	3.80

Table 4

Summary of thedata of band positions (in cm^{-1}) of various structural units in FT–IR spectra of $Li_2O–Pb_3O_4–SiO_2:Ag_2O$ glasses. The values of the peak positions are measured to a precision of ±1 cm^{-1}.

Glass	Asymmetric stretching vibrations of O-Si-Obonds	Symmetric stretching vibrations of SiO_4 units	$Pb^{(IV)}$-O bond	PbO_4 units
A_0	992	774	578	461
A_1	1016	772	574	458
A_2	1026	769	568	454
A_3	1032	767	563	452
A_4	1036	764	556	449

Table 5

Summary of the data on a.c. conductivity and other parameters of Ag_2O doped $Li_2O-Pb_3O_4-SiO_2$ glasses.

Glass	Exponent s (± 0.01)	N(E_F) (x 10^{21}, eV^{-1}/cm^3) (± 0.01)	A.E. for conduction W_{ac} (eV) (±0.01)	A.E. for dipoles (eV) (± 0.01)	τ_M (μs) (at T= 190 °C) (± 0.01)	Spreading factor (rads) α' (± 0.01)
A_0	0.49	2.15	0.69	0.32	86.4	0.59
A_1	0.53	2.06	0.74	0.36	130	0.52
A_2	0.58	1.92	0.80	0.41	152	0.45
A_3	0.64	1.83	0.87	0.45	191	0.42
A_4	0.69	1.68	0.91	0.53	196	0.36

Table 6

A.c. conductivity of various glass systems doped with Ag_2O measured at I kHz and 200 °C

S.No.	Glass system	A,c, conductivity $(ohm\text{-}cm)^{-1}$	
1	Ag_2O doped Li_2O-Nb_2O_5-P_2O_5 glasses	$8.2 * 10^{-8}$	Ref. [28]
2	Ag_2O doped sodium antimonate glass ceramics	$7.5* 10^{-8}$	Ref. [44]
3	Ag_2O doped $LiF–V_2O_5–P_2O_5$ glass	$8. 2*10^{-8}$	Ref. [45]
4	$AgI–Ag_2O–V_2O_5$ glasses	$6.84 *10^{-6}$	Ref. [46]
5	AgI doped silver phosphate glass	$5.0 *10^{-7}$	Ref. [47]
6	Li_2O-Pb_3O_4-SiO_2: Ag_2O (A_4)	$8.64 * 10^{-8}$	Present work

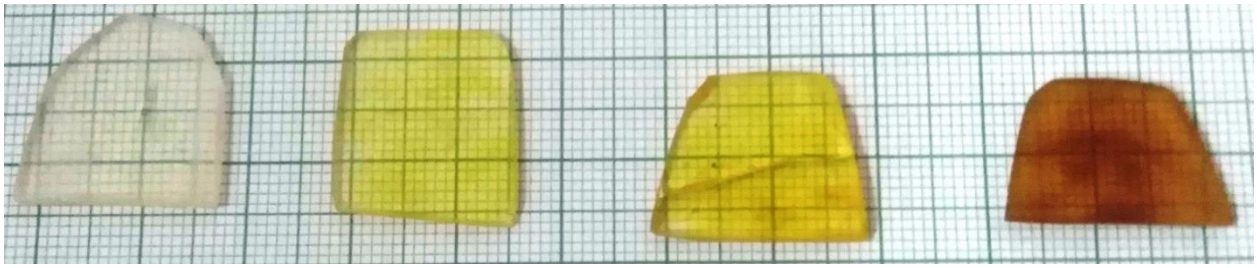

Fig. 1Photographs of the heat treated Li_2O-Pb_3O_4-SiO_2 glasses doped with different concentrations of Ag_2O.

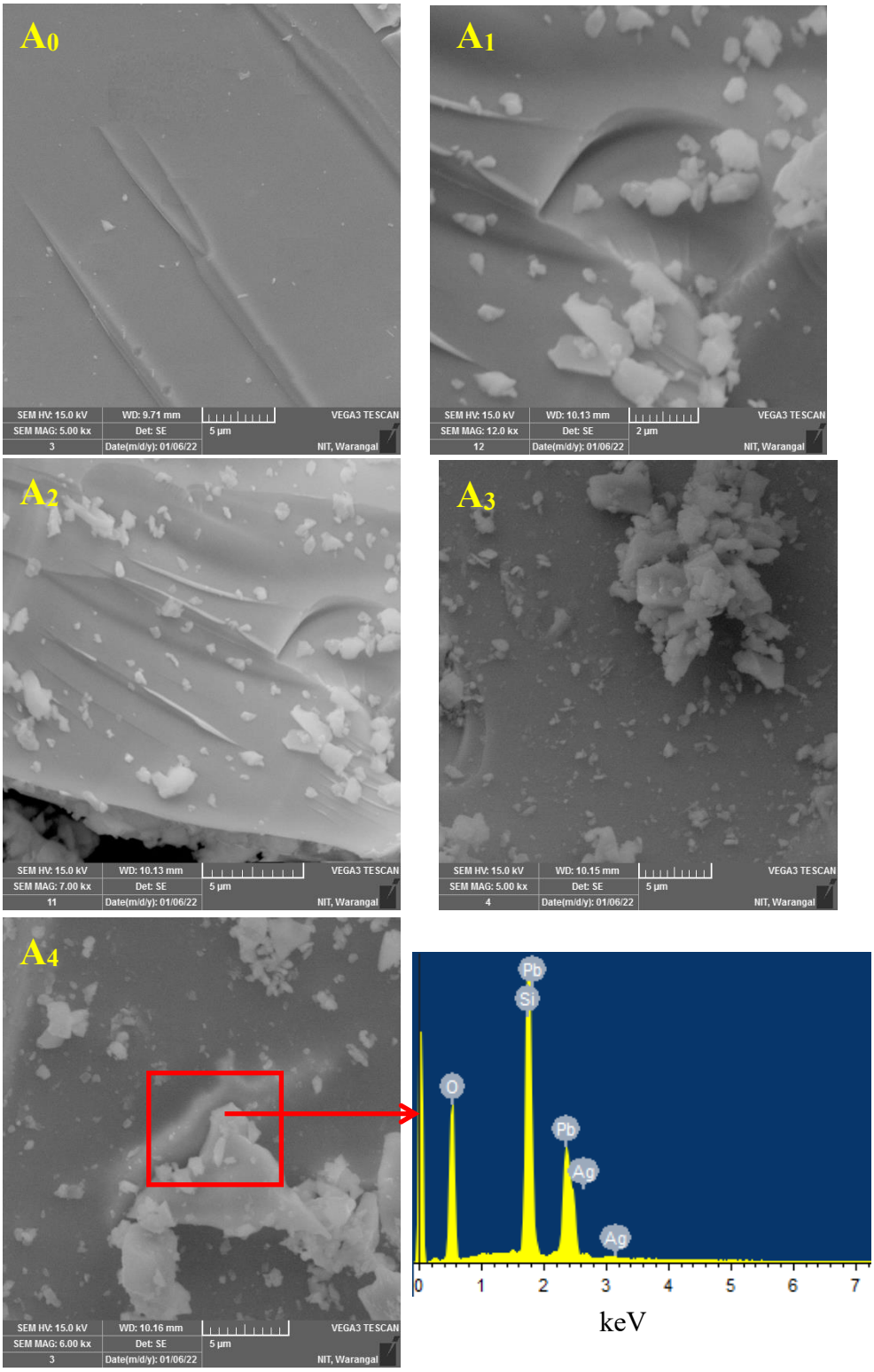

Fig. 2 SEM images of heat treated Li_2O-Pb_3O_4-SiO_2 glasses doped with different concentrations of Ag_2O. The figure also consists of EDS for the sample A_4.

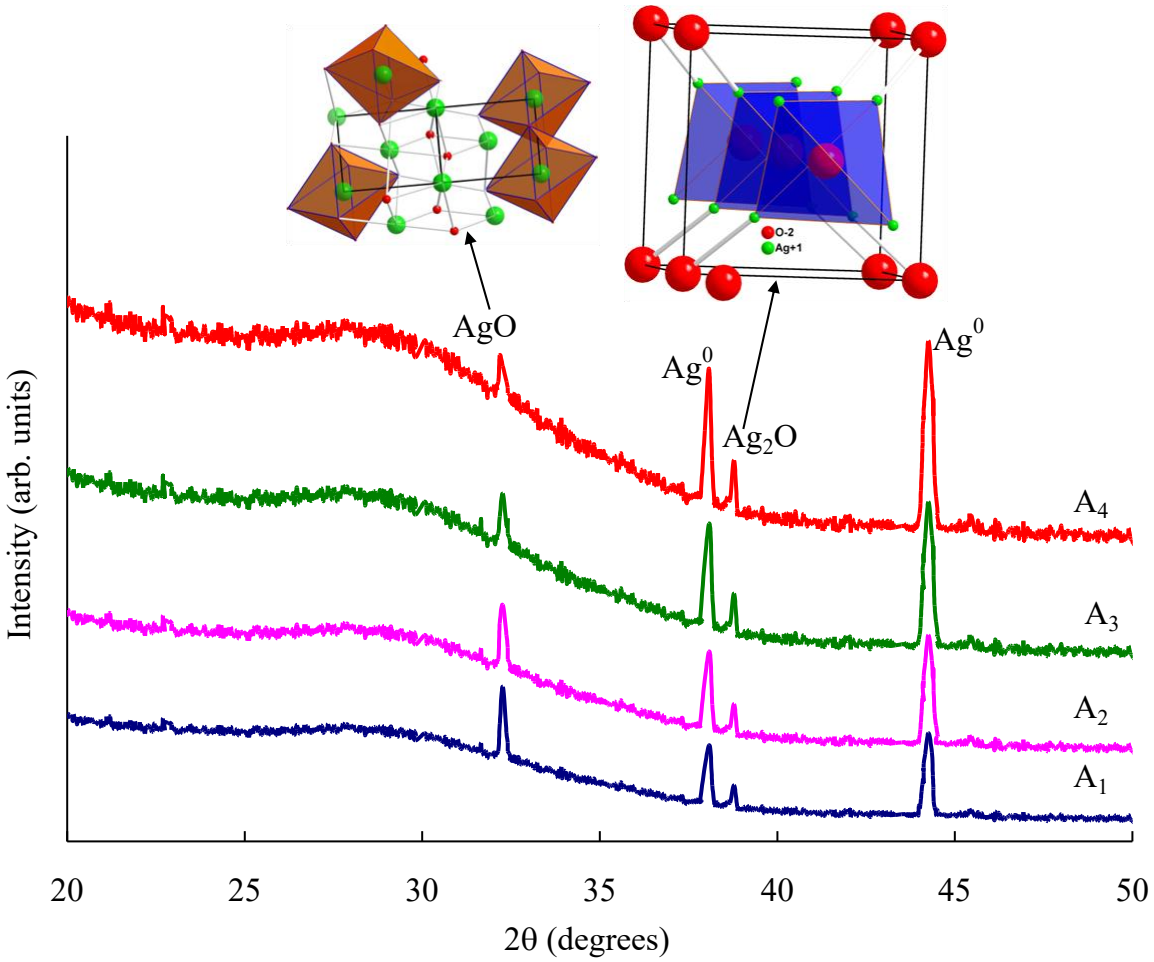

Fig. 3 XRD profiles of heat treated Li_2O-Pb_3O_4-SiO_2 glasses doped with different concentrations of Ag_2O.

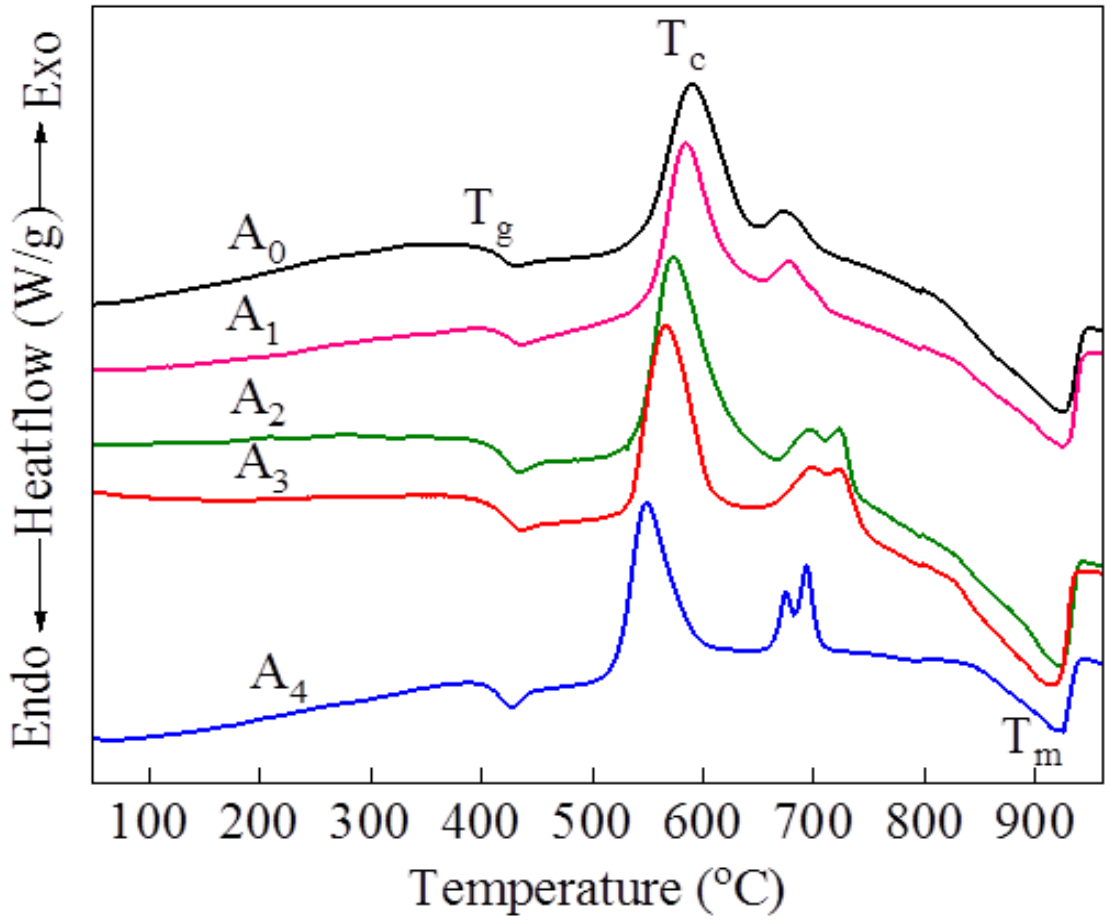

Fig. 4 DTA traces of heat treated Li_2O-Pb_3O_4-SiO_2 glasses doped with different concentrations of Ag_2O.

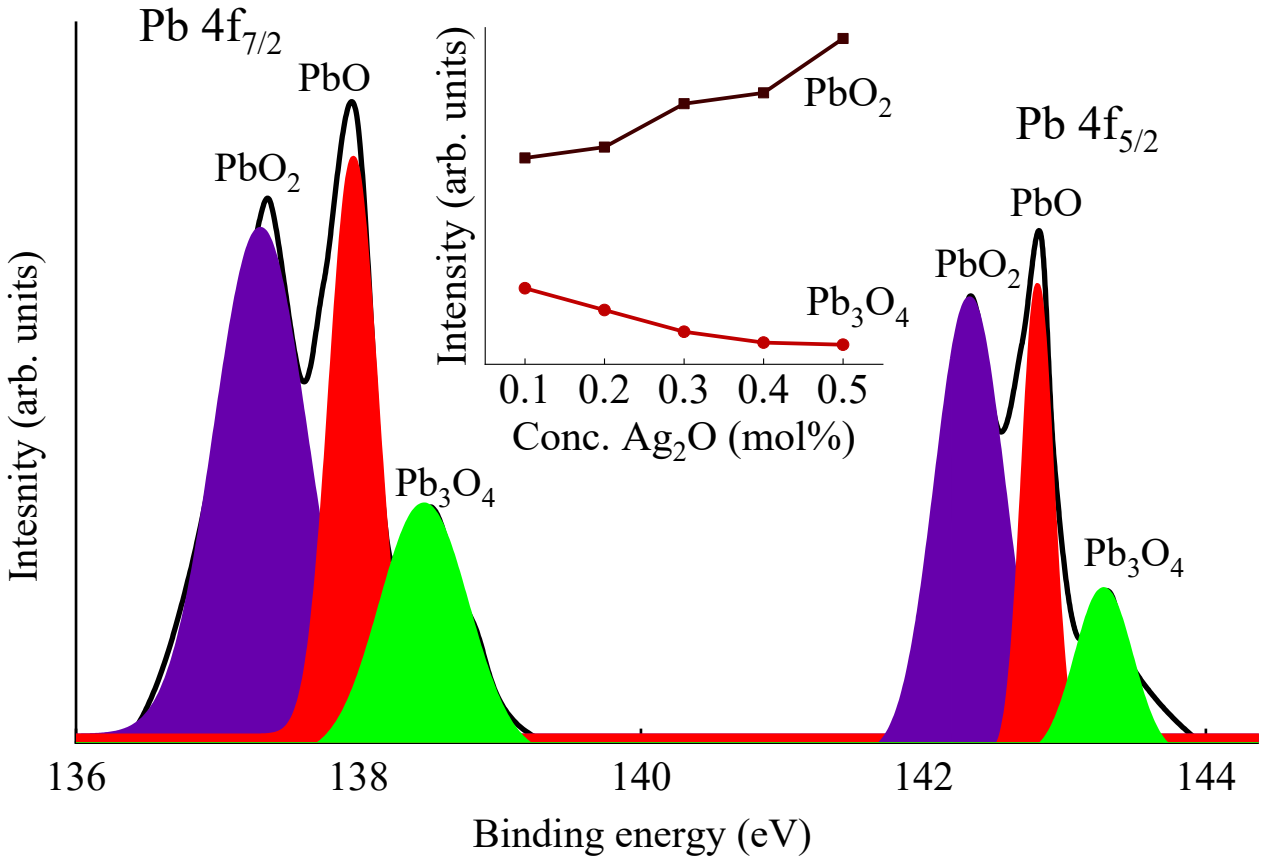

Fig. 5 Deconvoluted and fitted XPS spectra of PbO, PbO_2 and Pb_3O_4 in the glass sampleA_2 and inset represents the intensity variation of PbO_2 and Pb_3O_4 ($4f_{7/2}$) with the concentration of silver oxide.

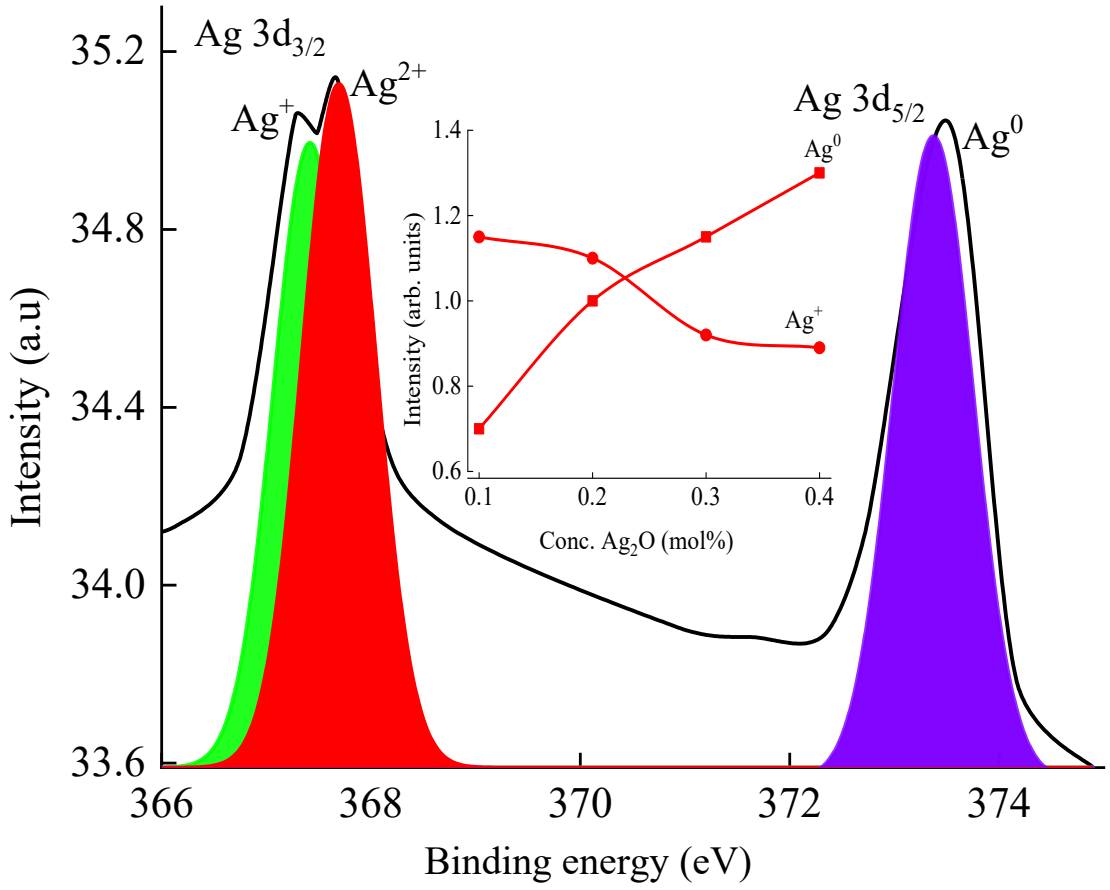

Fig. 6 Deconvoluted and fitted XPS spectra of Ag^0 and Ag^+ ions in the glass samples A_2 and the insets represents the intensity variation of Ag^0 and Ag^+ ions with the concentration of silver oxide.

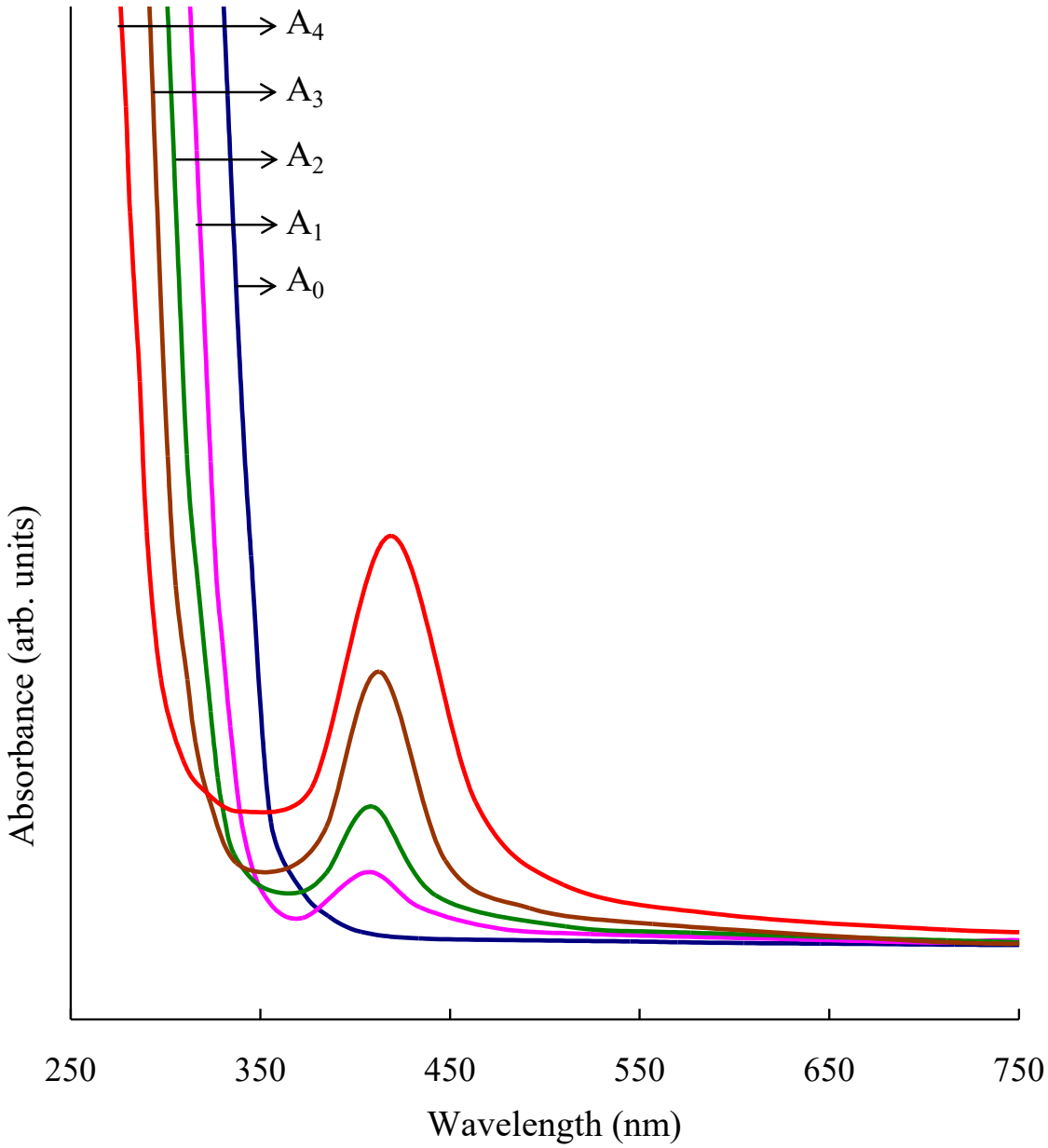

Fig. 7 Optical absorption spectra of Li_2O-Pb_3O_4-SiO_2 glasses doped with different concentrations of Ag_2O recorded after heat treatment.

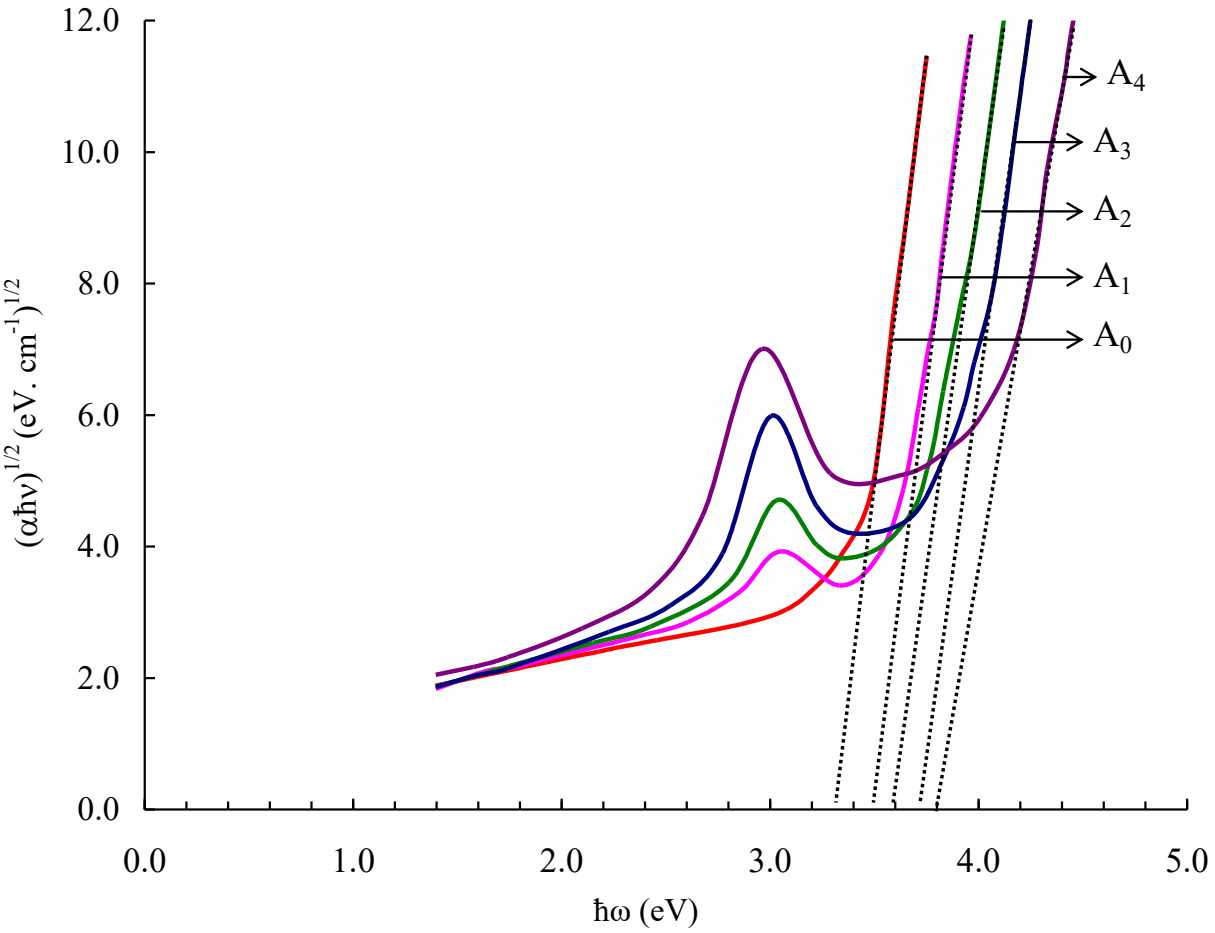

Fig. 8 Tauc plots of heat treated Li_2O-Pb_3O_4-SiO_2 glasses doped with different concentrations of Ag_2O.

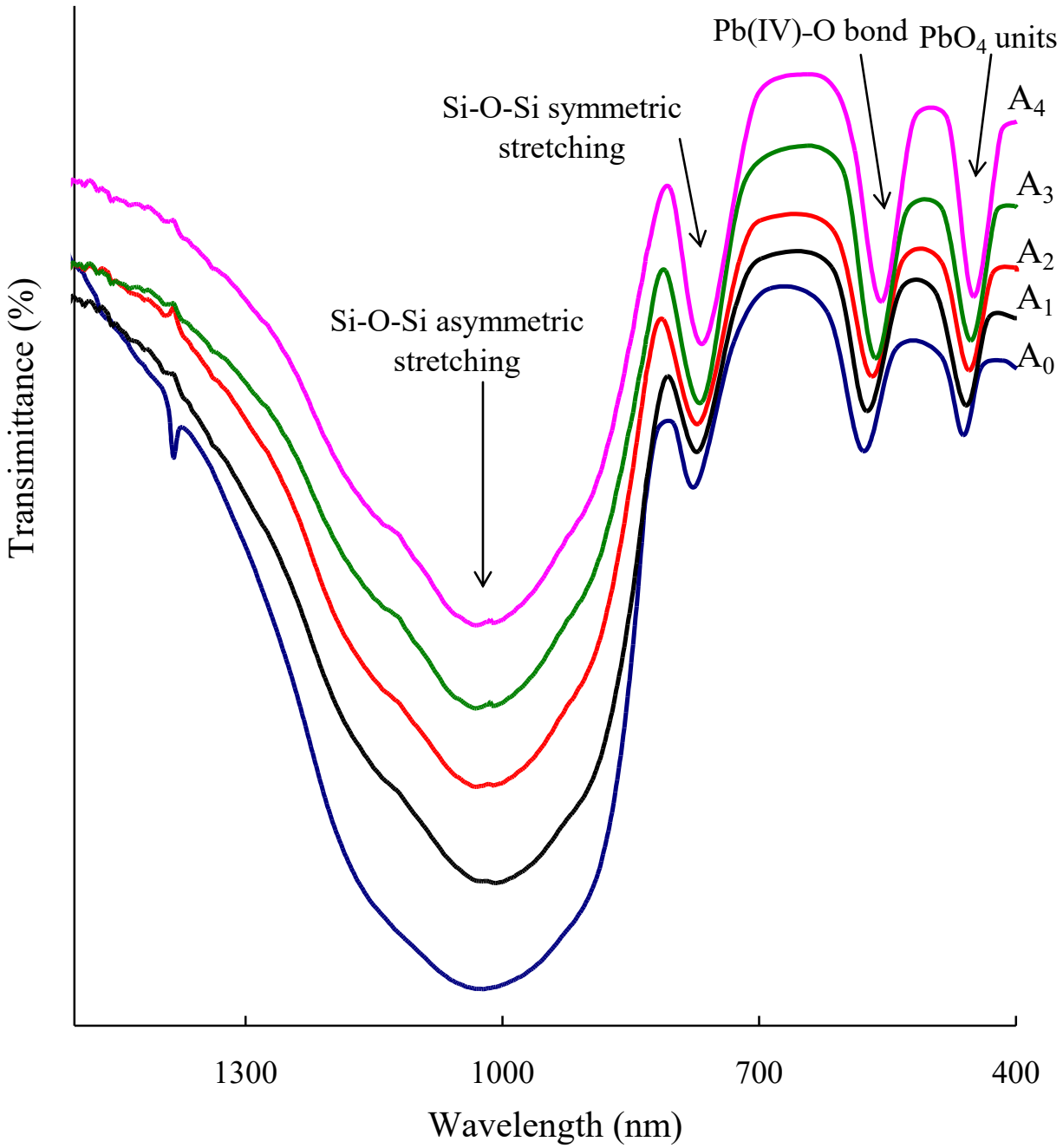

Fig. 9 FT-IR spectra of heat treated Li_2O-Pb_3O_4-SiO_2 glasses doped with different concentrations of Ag_2O.

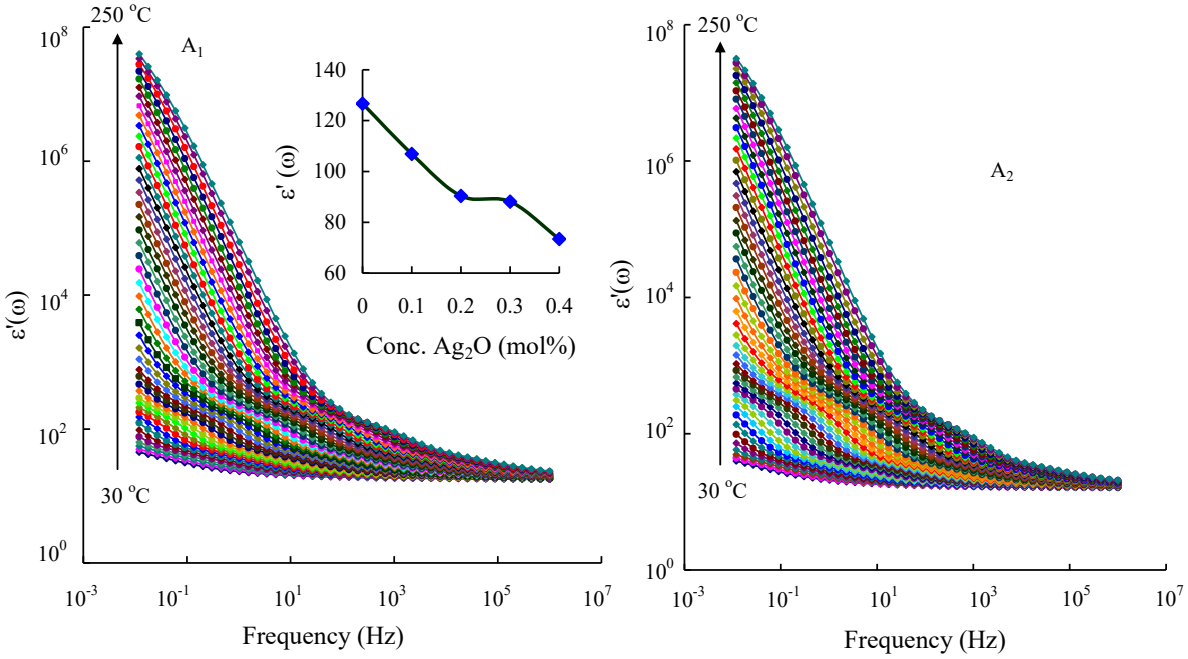

Fig. 10 (a) Variations of dielectric constant with frequency measured at different temperatures for the sample A_1 and A_2.

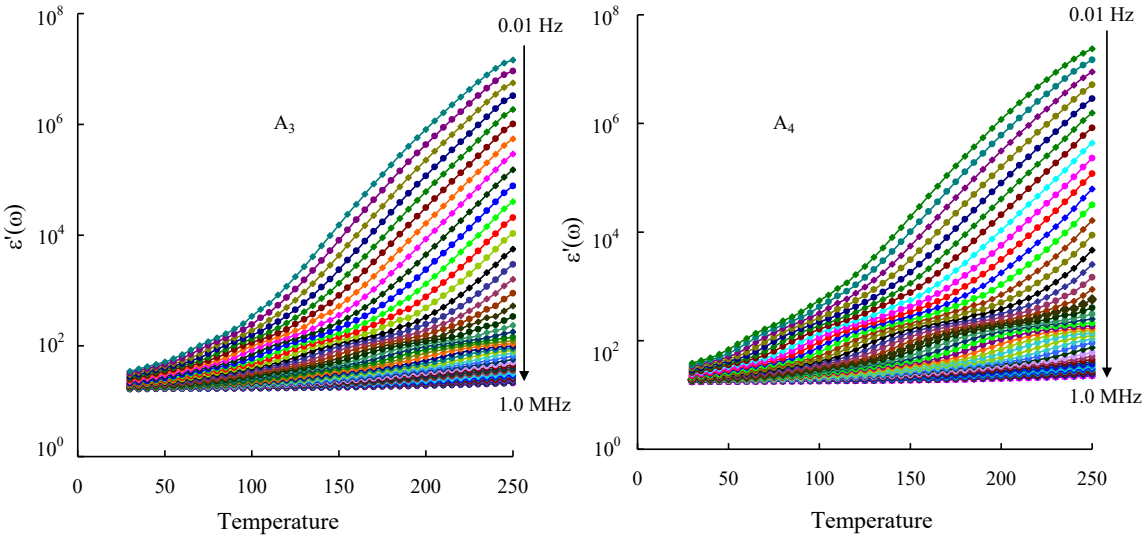

Fig. 10 (b) Variations of dielectric constant with temperature measured at different frequencies for the sample A_3 and A_4.

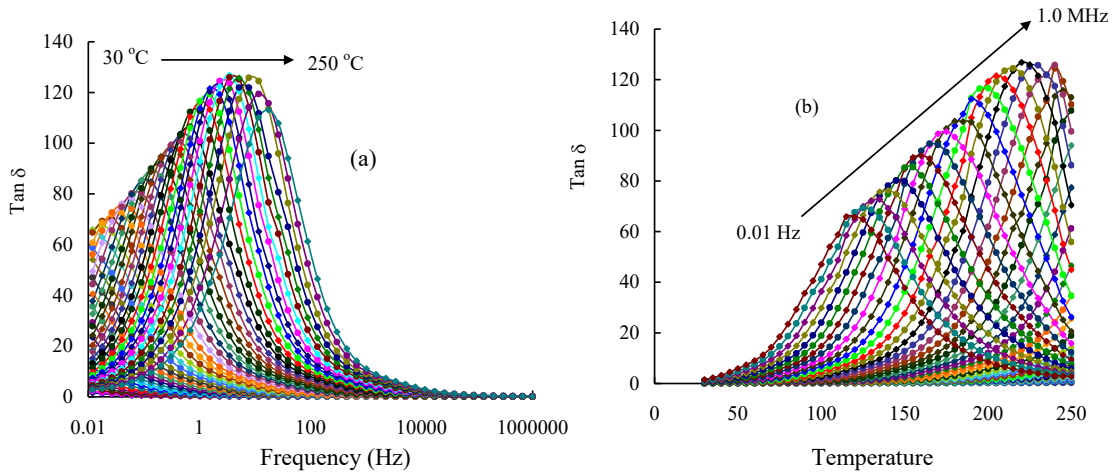

Fig. 11 Variations of dielectric loss (a) with frequency measured at different temperatures and (b) with temperatures for the sample A_4.

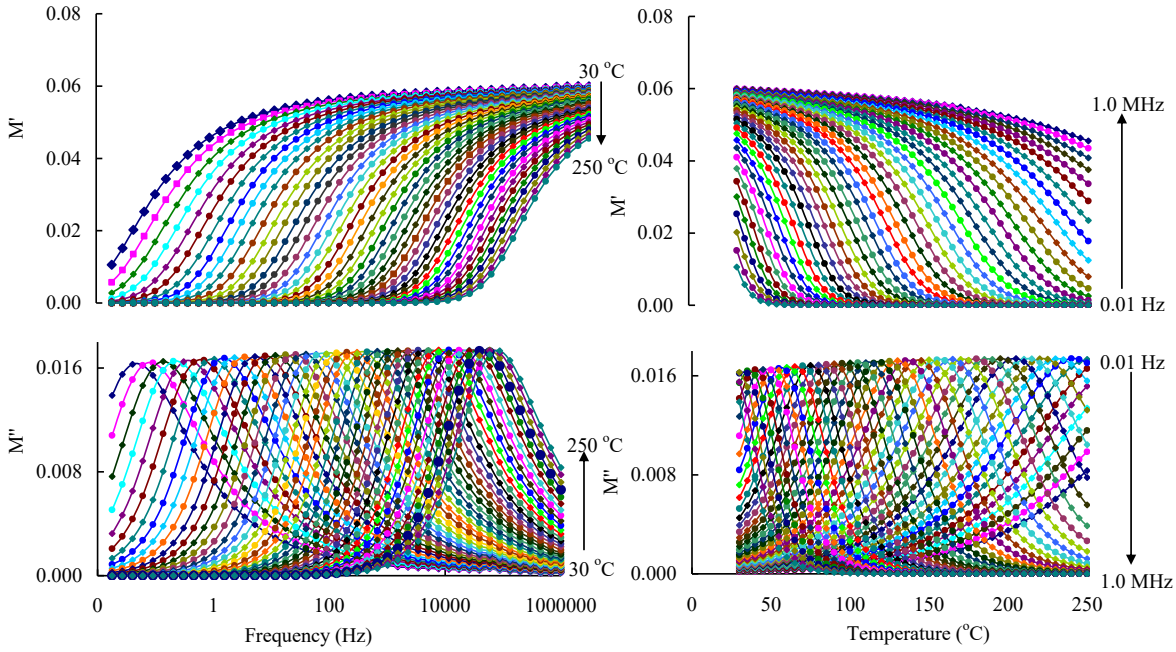

Fig. 12 Variations of electric moduli M′ and M″ (a) with frequency at different temperatures and (b) with temperature at different frequencies for the sample A_3.

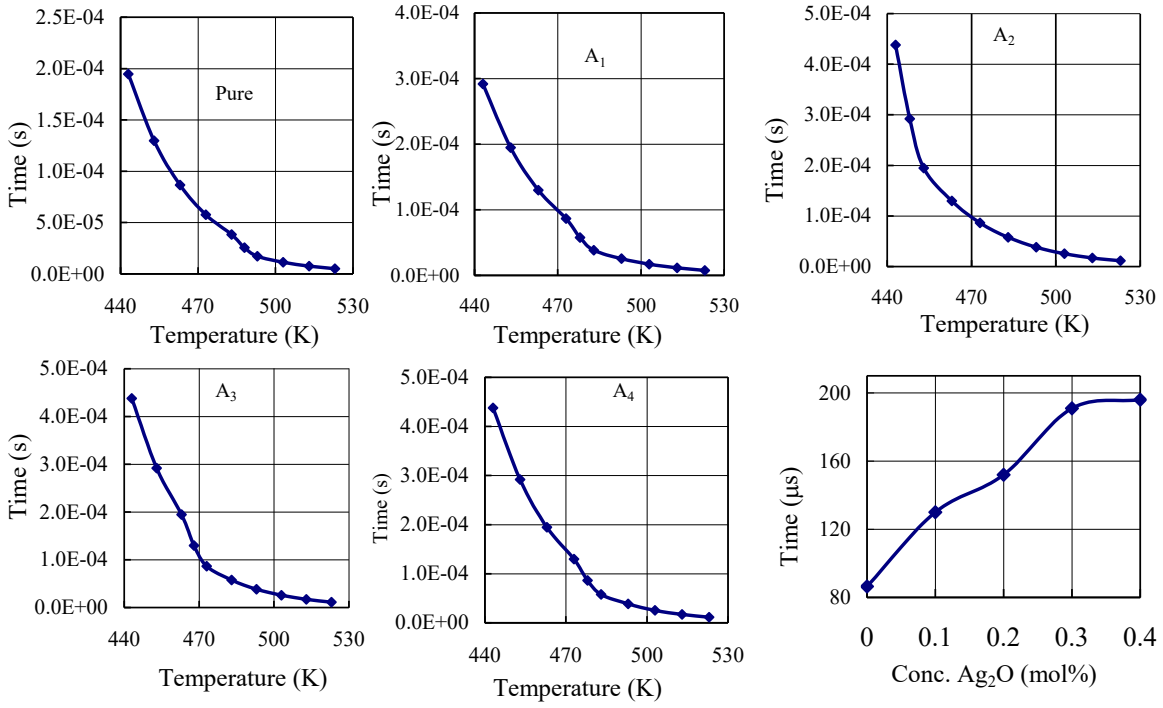

Fig. 13 The plots of relaxation times *vs* temperature for Li_2O-Pb_3O_4-SiO_2 glasses doped with different concentrations of Ag_2O.In this figure the variations of τ evalauted at 470 K with the concentration of Ag_2O is also presneted.

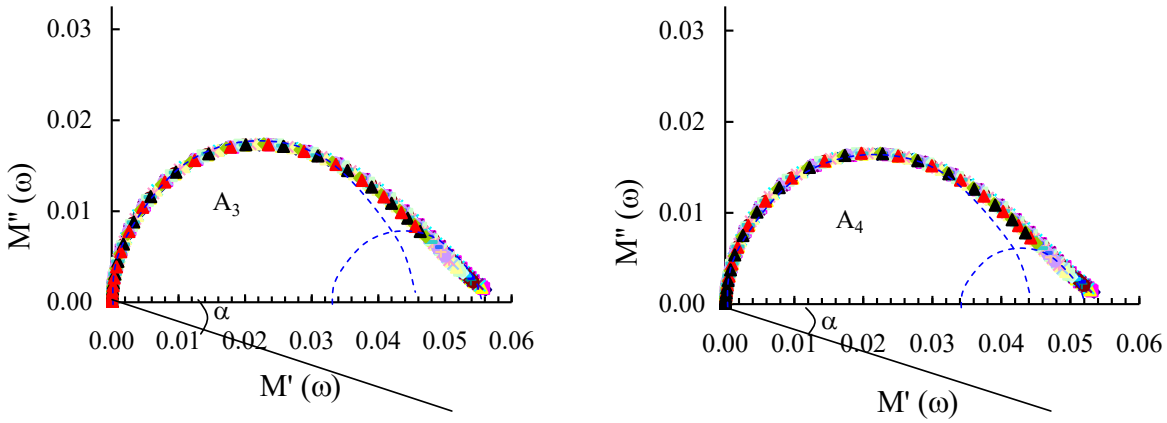

Fig. 14 Cole-cole plots for the samples A_3 and A_4.

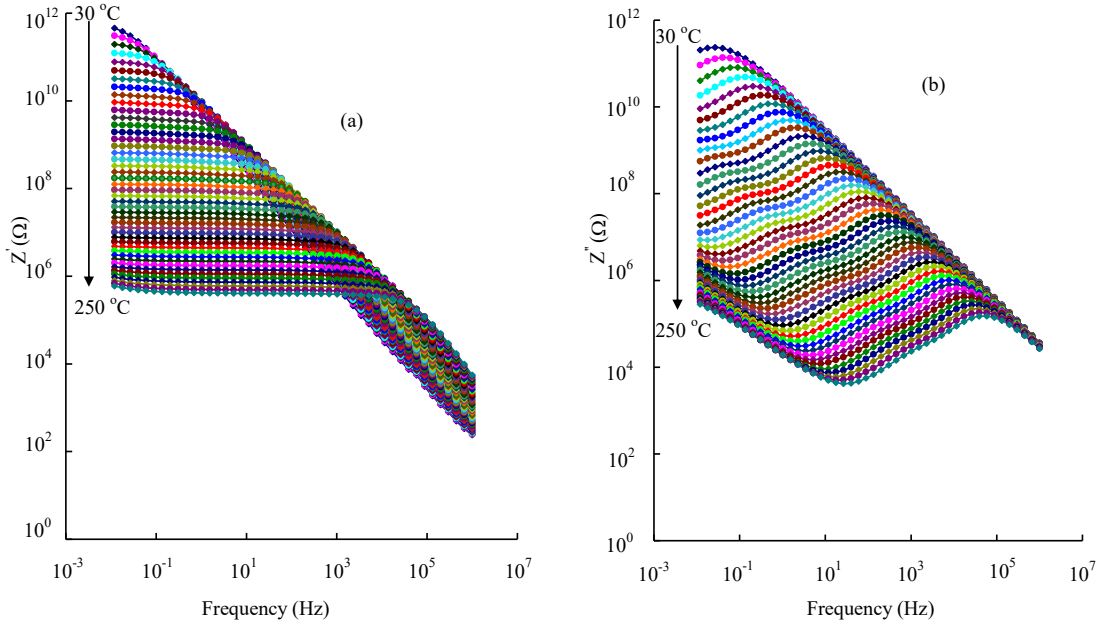

Fig. 15 Variations of Z' *vs* Z'' with frequency at different temperatures for the samples A_2.

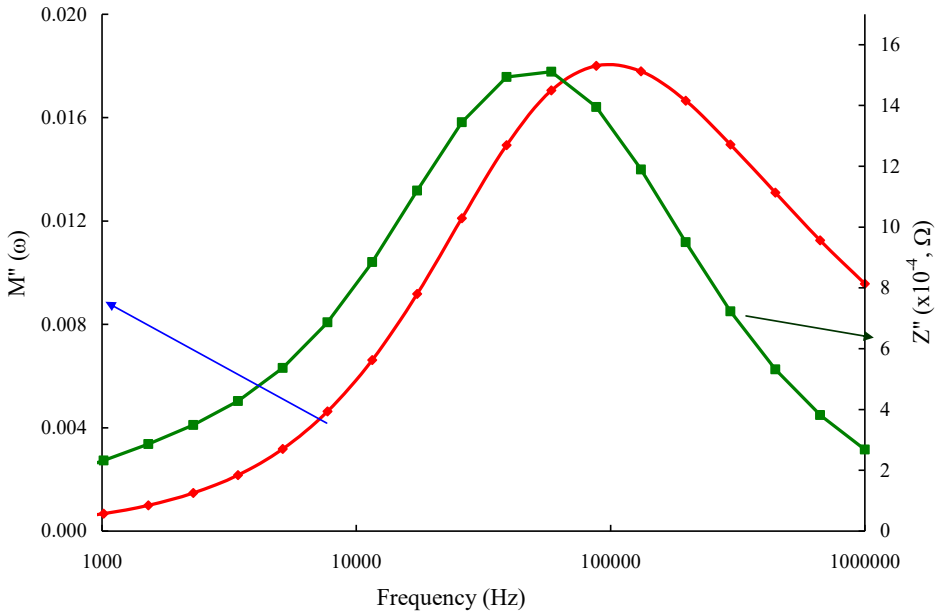

Fig. 15(c) Variation of M″ (ω) and Z″(ω) with frequency at 200 °C for the glass A_2.

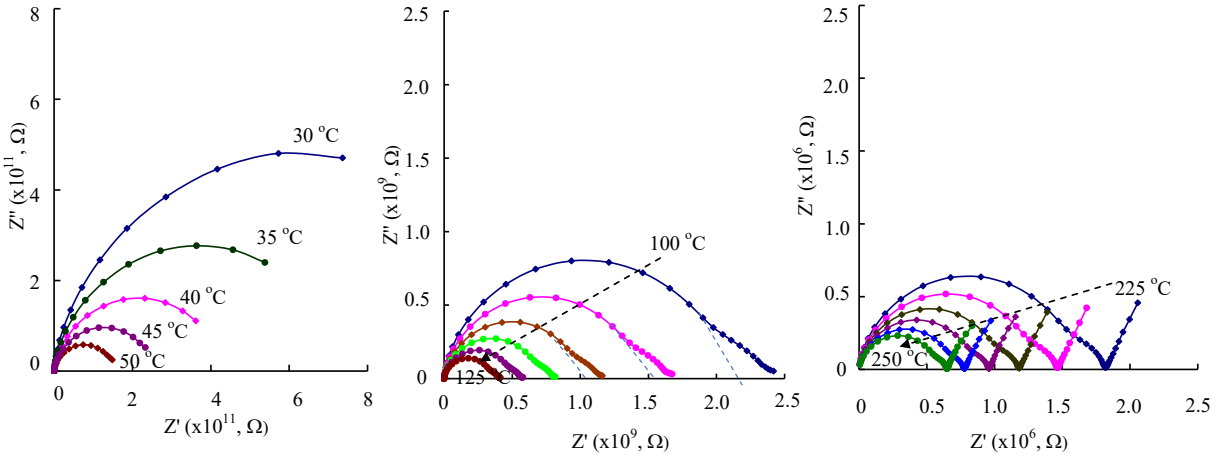

Fig. 16 (a) The plots of Z′ vs Z″ drawn in the temperature regions (b) 30-50 °C (b) 100-150 °C (c) 225-250 °C for the sample A_4.

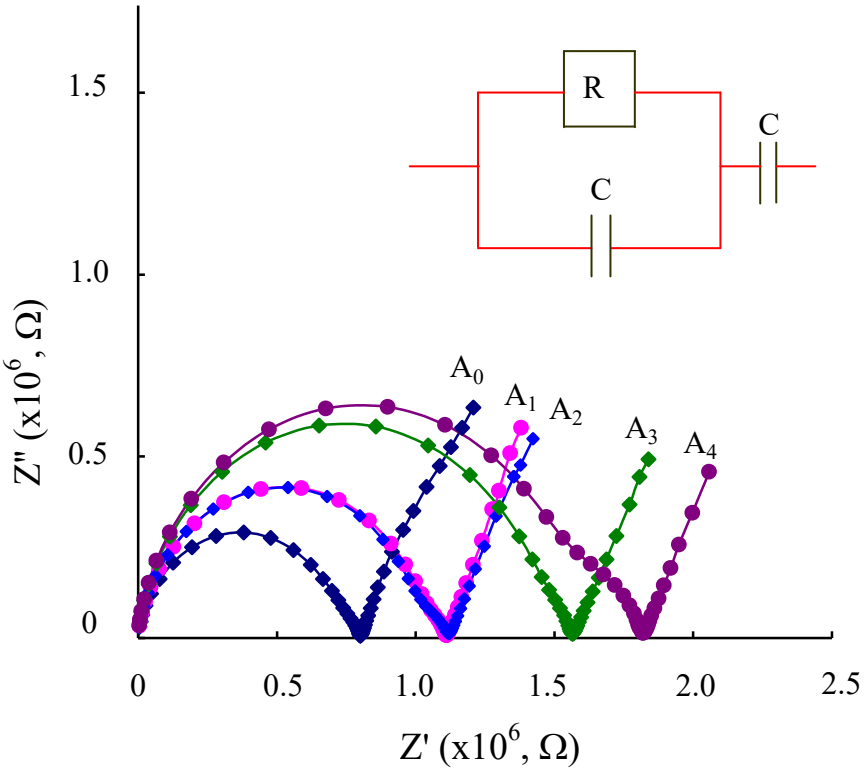

Fig. 16(d) The comparison plots of impedance of temperature of Li_2O-Pb_3O_4-SiO_2 glasses doped with different concentrations of Ag_2Odrawn at 250 °C. In the equivalent circuit diagram the parallel CR circuit accounts for semi-circular path of the diagram whereas additional series capacitor represents the inclined spur part.

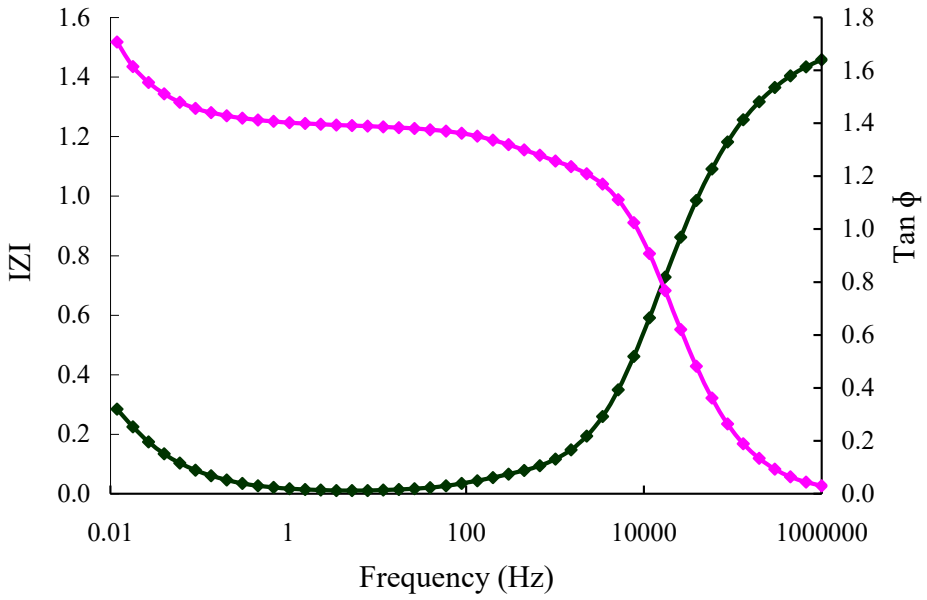

Fig.16(e) Bode plots (plots of total impedance $|Z|$ and the phase angle, $\tan\varphi = Z''/Z'$ *vs* ω) for a selected glass sample A_4 drawn at 200 °C.

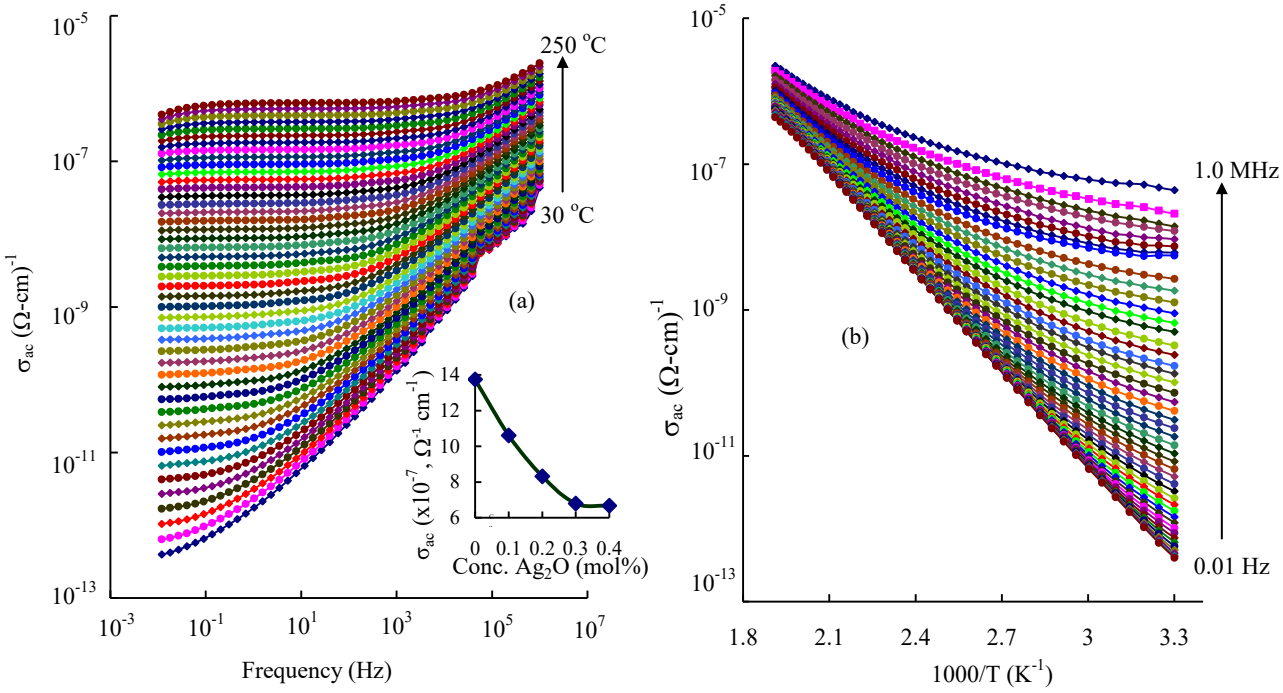

Fig. 17 The plots of σ_{ac} (a) vs frequency drawn at different temperatures and (b) *vs* 1/T drawn at different frequencies for the glass samples A_4. Inset represents the variation of σ_{ac} with concentration of Ag_2O measured at 250°C and 1 kHz.

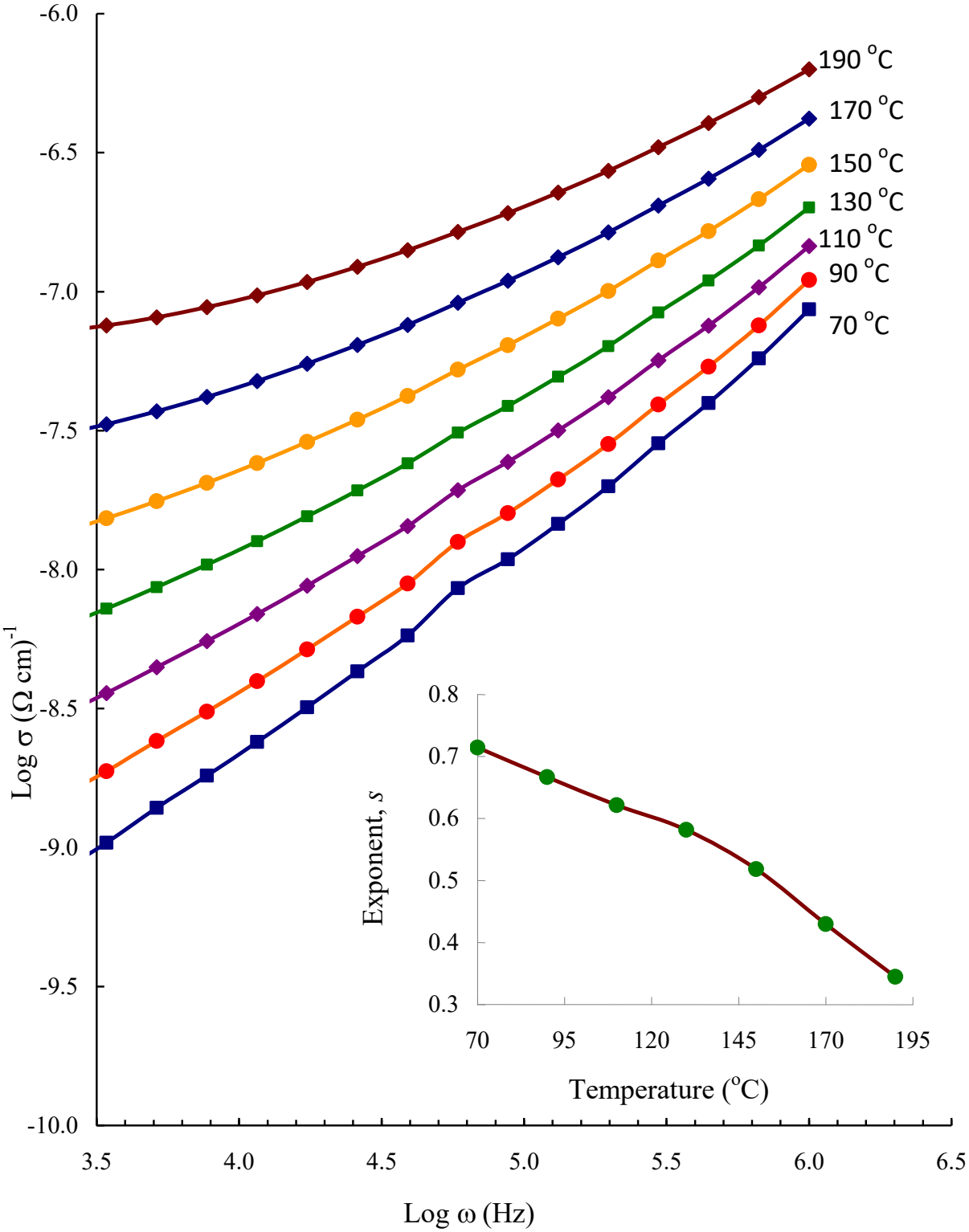

Fig. 18 Plots of log $\sigma_{ac}(\omega)$ versus log ω for the glass sample A_2drawn at different temperatures and to evaluate frequency exponents.